universe

MDPI

Review

Neutrino Telescopes and High-Energy Cosmic Neutrinos

Andrea Palladino [1], Maurizio Spurio [2,3] and Francesco Vissani [4,5,*]

1 Deutsches Elektronen-Synchrotron (DESY), Platanenallee 6, D-15738 Zeuthen, Germany; andrea.palladino@desy.de
2 INFN-Sezione di Bologna, Viale Berti-Pichat 6/2, 40127 Bologna, Italy; maurizio.spurio@bo.infn.it
3 Dipartimento di Fisica e Astronomia, dell'Università, Viale Berti Pichat 6/2, 40127 Bologna, Italy
4 INFN, Laboratori Nazionali del Gran Sasso, 67100 L'Aquila, Italy
5 Gran Sasso Science Institute, 67100 L'Aquila, Italy
* Correspondence: vissani@lngs.infn.it; Tel.: +39-346-73-28-009

Received: 23 December 2019; Accepted: 6 February 2020; Published: 10 February 2020

Abstract: In this review paper, we present the main aspects of high-energy cosmic neutrino astrophysics. We begin by describing the generic expectations for cosmic neutrinos, including the effects of propagation from their sources to the detectors. Then we introduce the operating principles of current neutrino telescopes, and examine the main features (topologies) of the observable events. After a discussion of the main background processes, due to the concomitant presence of secondary particles produced in the terrestrial atmosphere by cosmic rays, we summarize the current status of the observations with astrophysical relevance that have been greatly contributed by IceCube detector. Then, we examine various interpretations of these findings, trying to assess the best candidate sources of cosmic neutrinos. We conclude with a brief perspective on how the field could evolve within a few years.

Keywords: neutrino astronomy; neutrino telescopes; cosmic ray sources; multimessenger astrophysics

1. Introduction

1.1. Historical Notes

The search for high-energy neutrinos from the cosmos is closely linked to cosmic rays and particle physics. In fact, cosmic ray collisions produce particles from whose decays the neutrinos are born, mainly charged pions and muons. So, the roots of high-energy neutrino astronomy are linked to the names of Hess, Pacini, Pauli, Fermi, Yukawa, Anderson, Neddermeyer, Powell, Lattes, Occhialini and other famous physicists of the early 20th century.

History begins with a handful of theoretical works. In the middle of the Cold War, two independent papers [1,2] proposed to the scientific communities of the opponent countries the (same) idea, namely, of building high-energy neutrino telescopes. This is why the birth of this field of research is often attributed to these two works, but earlier explorations had been conducted in a Diploma thesis presented in 1958 at Moscow State University by Zheleznikh, by the time a student of Markov: see [2,3]. In this thesis it is written "It is worth searching for high energy neutrinos from Outer Space, especially, if the high energy γ-rays beyond the atmosphere were found" [3]: in other words, a very close connection between neutrinos and high-energy gamma rays was expected from the very beginning, because of the associated and inevitable production of charged and neutral pions. Incidentally, the study of gamma-ray radiation began in the same years by the paper of Morrison [4] (who mentions "the still unexploited neutrino channel", even if only in connection to stellar processes) and it is one of the most interesting branches of astronomy today. We cite the inspired words from

Reference [1]: "one may predict that these fields of high-energy quantum and neutrino astronomy will be opened up in the near future" which are particularly interesting, as nowadays there is occasionally still some resistance in accepting the consistence of "neutrino astronomy".

The first experimental searches for high energy neutrinos were conducted soon later by two experiments (KGF in India and CWI in South Africa, which were attended by scientists from all over the world, including the host countries, USA and USSR, UK, China and Japan) who released their final results in the beginning of the 1970s [5–7] and revealed for the first time atmospheric neutrinos but did not find evidence of other components in their dataset. Shortly afterwards the idea emerged of building a much larger detector, about a kilometer in size, as the way to proceed in the search for high-energy neutrinos from the cosmos. This led to the proposal of one experiment named DUMAND, carried out by scientists from USA and USSR; however, the well-known geopolitical circumstances prevented its realization. The first detector that succeeded in this goal has been IceCube, which built upon the experience of AMANDA, 1996–2005. In 2013, IceCube showed the first evidence of a new component of cosmic neutrinos [8], whose nature, however, is not yet identified.

For further historical discussion, see Reference [9–11].

1.2. Plan of This Review

The plan of this review paper is as follows: we begin by expounding the general expectations on cosmic neutrinos; next, we describe the principles of neutrino telescopes; we outline the possible signals and the background processes; then, we summarize the main observational results that have astrophysical significance; finally, we consider a few specific astrophysical models, as possible interpretations of these findings. In fact, even though numerous theoretical proposals preceded the discovery, it does not seem fair to say that the theory provided a solid guide to the discovery.

However, before proceeding in the discussion, it seems useful to conclude this brief introduction by highlighting a last momentous point, namely the discovery of the phenomenon of neutrino oscillations, anticipated in the decade 1957–1967 by Pontecorvo's theories [12] and fully accomplished thanks to a long series of experiments, including the Neutrino Detector Experiment in the Kamioka mine (Super-KamiokaNDE) in Japan and the Sudbury Neutrino Observatory (SNO) in Canada recognized by the Nobel prize in Physics in 2015 [13]. As this aspect has direct implications on the field of cosmic neutrinos of very high energies, and it seems to be one of the most reliable points in the theoretical interpretation, we will discuss in detail here.

2. High-Energy Neutrinos in the Cosmos

2.1. The Cosmic Ray Connection

It is widely believed that certain cosmic sources produce high-energy neutrinos. The simplest reason is just the knowledge of *atmospheric neutrinos,* that originate from cosmic ray interactions with Earth's atmosphere. Many variants of the known mechanism, which could lead to a potentially observable population of *cosmic neutrinos,* can be imagined. However, the reference picture for the production of high energy neutrinos is simply that, the same sites where cosmic rays are accelerated - or the environment that surround them—if endowed with sufficient target to convert a fraction of the energy into secondary particles, are potentially observable sources of high energy neutrinos.

Therefore, neutrino astronomy could be ultimately a major avenue to discover the sources of cosmic rays, which are still a matter of theoretical speculation and to date not yet sufficiently known. For this reason, we begin by collecting the main important facts on cosmic rays.

It is useful to recall some important observational facts concerning cosmic rays. The observation of high-energy part of cosmic ray spectrum at Earth allows us to distinguish several pieces, continuously connected but different among them. The flux is characterized by four main energy intervals: (1) the part below the *knee* at about $E_{\rm knee} \sim 3$ PeV; (2) the part just above, till the feature called the *ankle,* which is at about $E_{\rm ankle} \sim 5$ EeV; (3) the subsequent decade of energies; (4) the (GZK) *suppression* region,

which corresponds to the end of the observed spectrum. In all these regions, except the last one the distribution can be roughly described as **power laws,** namely by energy distributions of the form:

$$\Phi_{\rm CR} \sim E_{\rm CR}^{-\alpha}\,, \tag{1}$$

which are the characteristic features of the occurrence of (highly) non-thermal processes. The parameter α is called *the slope.* The observed slopes in the different energy intervals are not directly related to the slope at production; effects of propagation and/or of escape are plausibly also energy dependent. Indeed, the mechanisms of cosmic ray accelerations—for example, the Fermi mechanism—are expected to produce in several cases a distribution with slope $\alpha \sim 2$ until the maximum energy they can reach, which depends upon the accelerator.

A few general references are helpful for deepening the study including References [14,15] and the reviews in References [16–23]. For a discussion of the very important link with cosmic rays (briefly examined in this section) see References [17,24–27].

2.2. The pp and pγ Mechanisms of Neutrino Production

We assume that (most of) the observable cosmic neutrinos derive from astrophysical mechanism, that is, from cosmic ray collisions. Consider the case of very high energy protons (or nucleons) colliding over a nucleus $\mathcal{N}$ at rest, described approximately as an assembly of nucleons. This collision will lead to the production of many π^+, π^-, π^0, roughly in similar amount that we can resume symbolically by:

$$p + \mathcal{N} \to X + \text{many} \times (\pi^+ + \pi^- + \pi^0). \tag{2}$$

The experimental observation shows that the highest energy pion (called the leading pion) carries on average 1/5 of the initial kinetic energy of the proton—see for example, Reference [28,29]. Its decay will eventually lead to high-energy neutrinos and gamma rays:

$$\pi^0 \to \gamma + \gamma \text{ and } \pi^\pm \to \mu^\pm + \overset{(-)}{\nu}_\mu\,, \text{ followed e.g., by } \mu^+ \to e^+ + \nu_e + \bar{\nu}_\mu. \tag{3}$$

The kinematic of these decays is such that, in the decay of the neutral π^0, each gamma rays carries 1/2 of the initial energy, and likewise, in the decay chain of the charged leptons, anyone of the four light (anti)leptons carries away 1/4 of the initial energy (this corresponds to the result of the accurate calculation [30]; see also Appendix A). Thus, we have the very simple and useful rule of thumb:

$$E_\nu \sim \frac{E_\gamma}{2} \sim \frac{E_\pi}{4} \sim \frac{E_p}{20}\,. \tag{4}$$

Interestingly, this remains unchanged also for a completely different case, when the target is replaced by (high-energy) gamma rays. In fact, consider the process:

$$p + \gamma \to \Delta^+ \to n + \pi^+ \text{ or alternatively } \to p + \pi^0. \tag{5}$$

By simple kinematic considerations, one obtains that, on average, the mesons carry away 1/5 of the initial kinetic energy; therefore, the same rule of thumb (4) applies. For instance:

$$E_\nu = 100\ \text{TeV} - 10\ \text{PeV} \text{ corresponds to } E_p \sim 2\ \text{PeV} - 200,\ \text{PeV}$$

which is the region above (or just around) the knee of the cosmic rays spectrum. Note that no electron antineutrinos are formed in the decay chain of Equation (5). These appear after oscillations (see Section 3.1) even if a relative shortage of $\bar{\nu}_e$ persists.

The two major mechanisms for high-energy neutrino production, discussed just above, are usually referred to as pp-mechanism (Equation (2)) and $p\gamma$-mechanism (Equation (5)). They can apply to

various situations in the cosmos. The interconnection between cosmic rays (CRs), γ-rays and neutrinos is sketched in Figure 1.

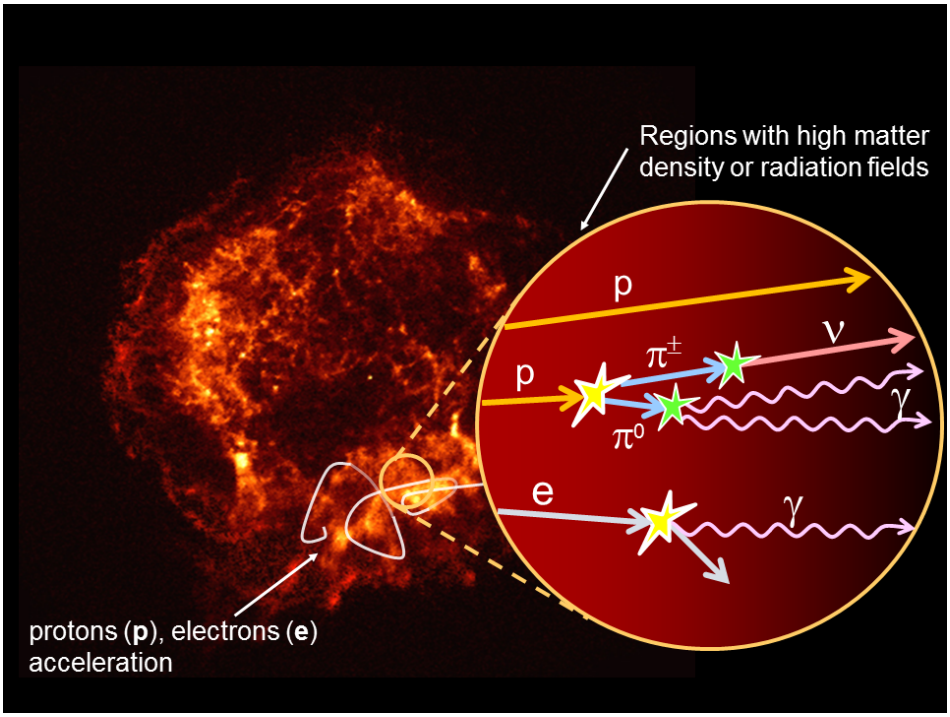


Figure 1. Astrophysical sources can accelerate CRs (protons, electrons and nuclei). A fraction of these particles diffuses outside the acceleration region, propagates in the galactic space (or intergalactic, if the source is external to the Galaxy) and can reach the Earth. Electrically charged cosmic rays do not travel in a straight line due to magnetic field deflections. Another fraction of accelerated protons (or nuclei) can instead interact with matter (pp-mechanism) or radiation fields ($p\gamma$-mechanism) surrounding the source. In this case, the decay of a neutral secondary particle (mainly π^0) produces a $\gamma\gamma$-pair, while the decay of charged particles (mainly $\pi^{\pm}$) produces (anti)neutrinos. The interaction of electrons with matter or radiation produces only γ-rays. Thus, the detection of neutrinos from the direction of a source is a unique way to find out what are the accelerators of protons and nuclei.

Let us examine now some differences between the pp- and the $p\gamma$-mechanism. The main ones concern the spectrum,

(i) The $p\gamma$-mechanism is a process with a defined threshold. For example, suppose having a photon target between the UV and X bands, say with energies of $\varepsilon \sim 0.1$ keV. For the production of a Δ-resonance, kinematics dictates:

$$E_p > \frac{m_\Delta^2}{4\varepsilon_\gamma} = \left(\frac{100\ \text{eV}}{\varepsilon_\gamma}\right) \times 4\ \text{PeV}, \tag{6}$$

which, according to (4), corresponds to neutrinos with minimal energy of $\sim$ 200 TeV (see also Reference [16]). In this production mechanism, the resulting neutrino (and very high-energy γ-ray) spectra will reflect the energy distribution of the target photons. If the interaction region moves at relativistic speeds with Lorentz factor Γ toward us, the observed neutrino energies are larger by a factor Γ^2, see e.g. [16,31].

(ii) The pp-mechanism is featured by a very important property of the hadronic interactions, namely the hypothesis of limiting fragmentation [32], to which we refer in the following as **scaling**. A detailed description of scaling variables, their definition, and the application on cosmic ray physics can be found in Reference [25]. According to the scaling, the secondary particle spectra

corresponds quite strictly to the primary distribution. Consequently, if the cosmic rays are power-law distributed, also the neutrinos and the very high-energy γ-rays will be power law distributed, with (almost) the same slope. One commonly says that, in this case, *the neutrino and gamma-ray spectra reflect the primary (cosmic ray) spectra*. In particular, if some variant of Fermi acceleration mechanism applies, we would have

$$\Phi_\nu \propto E_\nu^{-\alpha} \text{ with } \alpha \sim 2. \tag{7}$$

Other differences between the pp-mechanism and $p\gamma$-mechanism concern the proportions of the neutrinos and gamma-rays. Because a fraction of cosmic rays are nuclei, the pp-collision from individual nucleons in the nuclei will still produce neutrinos, where $p\gamma$-collisions will mostly lead to photo-disintegration which attenuates their energy [33]. The latter process reduces the production of secondary neutrinos. Finally, in the $p\gamma$-mechanism, a relatively larger amount of neutral pions is produced than for the pp-mechanism, yielding more γ-rays than ν's.

2.3. Connection of Neutrino and Gamma-Ray Astronomies

The pp- and $p\gamma$- production of secondary particles described in Section 2.2 is usually referred as the *hadronic* mechanism for γ-rays and ν production. However, a direct connection between high-energy neutrinos and γ-rays requires that certain assumptions be fulfilled. Differences arises from the fact that

- γ-rays can be produced also in the *leptonic* mechanisms in which only electrons are usually involved;
- γ-rays can be absorbed if the target is thick;
- when the γ-rays propagate for long distances, they are subject to absorption over background photons due to pair production

$$\gamma + \gamma_{\text{bkgr}} \to e^+ + e^- \,. \tag{8}$$

Concerning the last point, for instance, the opacity due to a thermal population with temperature T_{bkgr} and distributed over a region with size L is [34]:

$$\tau_{\text{pair}} = 1.315 \times \frac{L}{10\ \text{kpc}} \times f\left(\frac{E_\star}{E_\gamma}\right) \text{ with } \begin{cases} E_\star = m_e^2 / T_{\text{bkgr}} \\ f(x) \approx -3.68\, x\, \ln\left(1 - e^{-1.52\, x^{0.89}}\right). \end{cases} \tag{9}$$

Consider for example, the ubiquitous CMB photons such that $E_\star = 1.1$ PeV. If the distance of propagation is 100 Mpc and the energy is $E_\gamma = 100$ TeV, we expect a survival fraction of $\exp(-\tau_{\text{pair}}) = 28\%$; but also for a Galactic distance $L = 8.5$ kpc, a photon of $E_\gamma = 1$ PeV has $\exp(-\tau_{\text{pair}}) = 39\%$. Therefore, the attenuation effect is very important for propagation over extragalactic distances, but it is not negligible for the highest energy galactic cosmic rays. When the contribution of background infrared photons (due to *reprocessed* star light) is included, the Universe is expected to become opaque already at the TeV energy scale. Thus, at the highest energies, the connection between extragalactic gamma rays and neutrinos is indirect. Detailed numerical codes for the description of more complex situation where absorption occur are publicly available, see for example, those of `nuFATE` and `nuSQuIDS` codes in Reference [35].

On the contrary, there are various cases when the connection is much more direct. For instance, consider the case of young supernova remnants (SNRs), namely, the mass of gas expelled by a supernova. This is considered as a plausible candidate for the acceleration of (galactic) cosmic rays. Moreover, the regions where core collapse supernovae explode are also sites of intense stellar formation activity, and therefore, it often happens that SNRs are surrounded by large amounts of target material, see References [36,37] and compare with Reference [38] that focusses only on particle physics aspects instead. This is the case of the SNR denoted as RX J1713.7-3946, that is just 1 kpc from the Earth and it

is considered as a promising source of high energy neutrinos, whose neutrino flux can be predicted thanks to the observed gamma rays: see Reference [39] for a first discussion, Reference [40] for an accurate evaluation.

In general, considering this type of galactic source, we expect [41] a discernible signal in the neutrino telescopes of a 1 km^3-scale only if the γ-ray flux is larger than:

$$I_\gamma(> 10\,\text{TeV}) = (1-2) \times 10^{-13}\,\text{cm}^{-2}\,\text{s}^{-1}. \tag{10}$$

A detailed discussion of the signal of the neutrinos, derived following these principles from the γ-ray observations of certain specific galactic sources, can be found in Reference [42], see Figure 2 from this reference. There, it is shown that for the KM3NeT detector (see Section 4.2.3) an observation with 3σ significance is possible in about six years of operation for sources as RX J1713.7-3946 and Vela Jr.

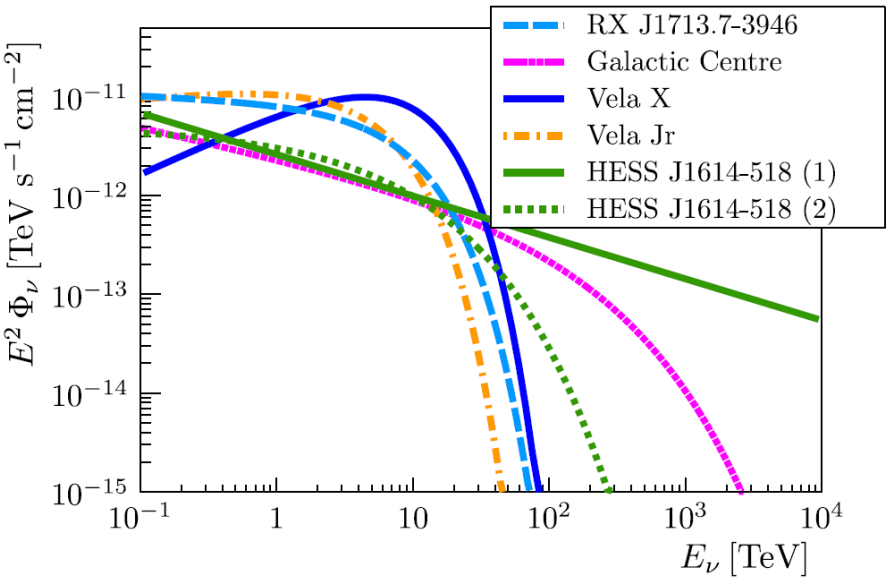


Figure 2. Prediction of the ν_μ fluxes for different galactic sources used in the sensitivity studies of the KM3NeT collaboration [42].

3. From Cosmic Neutrino Sources to the Earth

3.1. Effects of Neutrino Propagation

The relevance of neutrinos oscillations to the interpretation of cosmic neutrinos was remarked quite soon, see for example [43–45]. For instance, in Reference [44] we read "if neutrino oscillations occur and cause the transition $\bar{\nu}_e \rightleftarrows \bar{\nu}_\mu$, then the flux of $\bar{\nu}_e$ increases. This effect is particularly important for $p\gamma$ neutrinos" while in Reference [45] we read "if there exist more than two neutrino types with mixing of all neutrinos, cosmic neutrino oscillations may result in the appearance of new type neutrinos, the field of which may be present in the weak interaction hamiltonian together with heavy charged lepton fields." Actually, these observations still delimit the frontier of research in the field of cosmic neutrinos, for the reasons we recall here below and will elaborate in Sections 5.3 and 5.4.

The vacuum oscillation phases that have been probed in terrestrial experiments can be parameterized as:

$$\varphi = \frac{\Delta m^2\, L}{2E_\nu} = 3 \times 10^4\, \frac{\Delta m^2}{7.4 \times 10^{-5}\,\text{eV}^2}\, \frac{50\,\text{TeV}}{E_\nu}\, . \frac{L}{\text{pc}} \tag{11}$$

This means that vacuum oscillations have to affect neutrino propagating over cosmic distances. When we discuss astrophysical neutrinos, in the energy range between hundreds of TeV and multi-PeV,

produced by extragalactic sources (i.e., at least at distances of Mpc), the oscillation phase becomes order of 10^{10} or more. In this case the only observable and meaningful physical quantity is the phase averaged oscillation. The minimal setup to analyze the effect on cosmic neutrinos is just the average value of the vacuum probabilities when the oscillating phases are set to zero:

$$P_{\ell\to\ell'} = \sum_{i=1}^{3} |U_{\ell i}^2|\ |U_{\ell' i}^2|. \tag{12}$$

This limit, when the oscillation probabilities reduce to constant values, is known as *Gribov-Pontecorvo* regime [43]. Using the most recent best fit values of the mixing angles [46]:

$$\{\theta_{12}, \theta_{13}, \theta_{23}, \theta_{\rm CP}\} = \{33.82^\circ, 8.61^\circ, 48.3^\circ, 222^\circ\} \tag{13}$$

the resulting approximate values of the oscillation probabilities in Equation (12) correspond to:

$$\text{matrix}(P_{\ell\to\ell'}) = \begin{pmatrix} 0.548 & 0.185 & 0.267 \\ 0.185 & 0.436 & 0.379 \\ 0.267 & 0.379 & 0.354 \end{pmatrix} \text{ with } \ell, \ell' = \text{e}, \mu, \tau \tag{14}$$

Given a flavor fraction of different neutrinos at the source, f_ℓ^0, such that $0 \le f_\ell^0 \le 1$ and $f_{\rm e}^0 + f_\mu^0 + f_\tau^0 = 1$, one calculates the final flavor fraction at Earth as:

$$f_\ell = \sum_{\ell=\text{e},\mu,\tau} P_{\ell\to\ell'}\ f_{\ell'}^0. \tag{15}$$

(For a thorough investigation of the relevant parameters and an assessment of the uncertainties, see References [47,48].)

The major consequence of Equation (15) for cosmic neutrinos on Earth is that the spectra of the three neutrino flavors are approximately the same, if they have exactly the same power law distribution. This is particularly true in the case of muon and tau neutrinos, due to the parameters of oscillations, which display an approximate mu-tau exchange symmetry.

Assuming in fact that neutrinos originate from pp or $p\gamma$ production (Section 2.2). In astrophysical environments, the pion decay chain is complete (i.e., also the muon decays). According to Equation (3), one has exactly a $(\nu_\mu + \bar\nu_\mu)$ pair for each ν_e or $\bar\nu_e$, leading to flavor fractions at the source $f_{\rm e}^0 = 1/3$, $f_\mu^0 = 2/3$ and $f_\tau^0 < 10^{-5}$. In all large apparata used to study cosmic neutrinos, there is no experimental method able to distinguish reactions induced by a neutrino or an anti-neutrino; thus, no separation between particles and anti-particles can be made.

The flavor fractions can thus be written using a single parameter, $f = f_e^0$, as:

$$\{\, f_e^0, f_\mu^0, f_\tau^0 \,\} = \{f, 1-f, 0\}\ . \tag{16}$$

With oscillation parameters given in Equation (14), we obtain:

$$\{\, f_e, f_\mu, f_\tau \,\} = \{0.185 + 0.362f, 0.436 - 0.251f, 0.379 - 0.112f\} \tag{17}$$

that verify the properties mentioned just above. In particular, for $f = 1/3$ the flavor fractions are $1/3 + \{-0.027, +0.019, +0.008\}$, namely, they are very close to each other after oscillations.

Tau neutrinos, in this context of discussion, have a central role as they are not produced in charged mesons decay, either in atmospheric or astrophysical environments. The conventional component of atmospheric neutrinos from pion and kaon decays, as described in Section 6.1, is *mostly* composed by $\nu_\mu + \bar\nu_\mu$; at few 10-100 TeV one expects the onset of a new component due to charmed meson decays, that should instead be almost equally composed by electron and muon neutrinos (more discussion

below). Because at energy scales larger than 1 TeV atmospheric neutrinos are not significantly subject to oscillations in a path of length of the Earth diameter, we do not expect the presence of any atmospheric ν_τ. Instead it is for sure that cosmic neutrinos are subject to neutrino oscillations, and therefore tau neutrinos have to be present. The interpretation of tau neutrino events should be regarded with high confidence as due to high-energy neutrinos that have traveled upon cosmic distances. See Reference [49] for a quantitative and updated discussion of the expectations.

Note that, generally, neutrino and antineutrino events are not distinguishable and therefore are added together - the Glashow resonance events due to $\bar{\nu}_e$'s, discussed in Section 5.4, are an exception to this rule.

3.2. Neutrino Interactions in the Earth

The distance traveled by a neutrino in the Earth volume, before reaching the detector, is:

$$\ell(\theta_{\rm N}; d) = (R_\oplus - d)\cos\theta_{\rm N} + \sqrt{(R_\oplus)^2 - (R_\oplus - d)^2 \cdot (\sin\theta_{\rm N})^2}, \tag{18}$$

where $\theta_{\rm N}$ is the nadir angle, $R_\oplus = 6371$ km the average Earth radius. The quantity d represents the depth of the detector (of the order of a few km at most). The formula is derived from basic trigonometric considerations.

The Earth is not fully transparent to the highest energy neutrinos, due to the increase of the absorption cross section of the matter, $\sigma_{\rm abs}$, with the increase of the neutrino energy E_ν. The main contribution is due to the charged current (CC) interaction with nucleons $\sigma_{\rm abs} \simeq \sigma_{\rm CC}$ that can be modeled as deep inelastic scattering. The neutral current interaction produces a neutrino with a reduced energy, and this does not significantly affect the absorption cross section. Detailed calculations (performed also through Monte Carlo methods) can account for the deformation of the arrival energy spectrum due to neutral current interactions and due to the ν_τ regeneration effect [50]. The propagation of the $\bar{\nu}_e$ flavor at 6.3 PeV is also affected by the resonant formation of the W boson in $\bar{\nu}_e + e^-$ collisions, described in Section 5.4.

The absorption coefficient of the neutrinos, according to the usual formula $e^{-\tau}$, depends on the *opacity factor* τ, defined as:

$$\tau \equiv \sigma_{\rm abs}(E_\nu) \times z(\theta_{\rm N})\ . \tag{19}$$

Here, the *column density* $z(\theta_{\rm N})$, which corresponds to the number of nucleons per cm^2 that are crossed from a certain nadir angle, can be estimated by the formula

$$z(\theta_{\rm N}) = 2N_A \int_0^{R_\oplus \cos\theta_{\rm N}} \rho\left(\sqrt{x^2 + (R_\oplus \sin\theta_{\rm N})^2}\right) dx, \tag{20}$$

where N_A is the Avogadro number, x is the coordinate along the neutrino path inside the Earth. Here, we neglected d (and h) in the formula (18) for $\ell(\theta_{\rm N}; h, d)$, which is sufficient for our purposes. The terrestrial density as a function of the distance from the center $\rho(R)$, estimated using the PREM model [51] with an accuracy adequate to the current need, is shown in the left panel of Figure 3. One can define the inverse of the column density as the *critical value of the cross section*

$$\sigma_\star(\theta_{\rm N}) = 1/z(\theta_{\rm N}). \tag{21}$$

In fact, when the absorption cross section satisfies the condition $\sigma_{\rm abs}(E_\nu) = \sigma_\star(\theta_{\rm N})$, the opacity is $\tau = 1$ and the absorption coefficients is $1/e \sim 0.37$. The right panel of Figure 3 compares $\sigma_\star(\theta_{\rm N})$, depicted in blue and shown as a function of the nadir angle, with the cross section given for three values of the energy, indicated in the black lines. The angles at which the absorption coefficients of the neutrinos is $1/e$ are, 32° for $E_\nu = 100$ TeV, 59° for $E_\nu = 1$ PeV, 81° for $E_\nu = 10$ PeV. Therefore, at very-high energies, we receive neutrinos arriving only from a limited patch of the sky, close to the local horizon. Note that

the rotation of the Earth changes the region of the sky seen in the course of the day, except for the case of a detector located at the poles (such as IceCube) when this does not change.

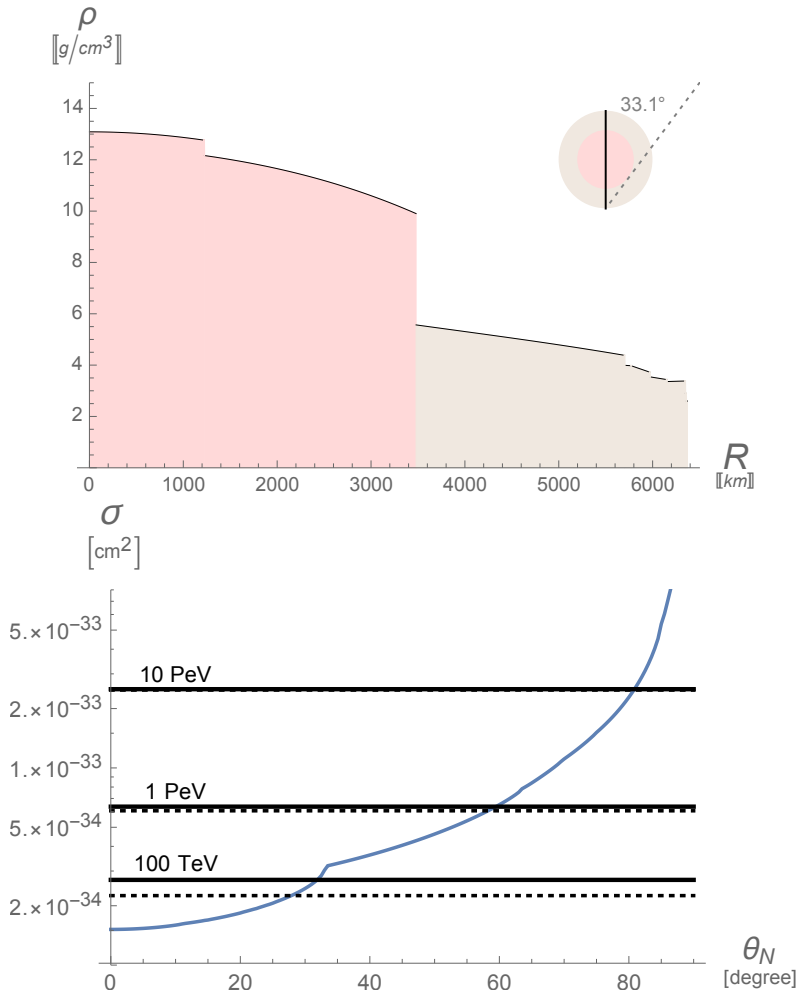


Figure 3. Top panel: Earth's density in g/cm^3 according to the PREM model [51]; note the discontinuity between the mantle (brown area) and the core (red area) at a distance from the center of $R_{\rm core} = 3840$ km. The limiting angle $\theta_{\rm N,core} = \arcsin(R_{\rm core}/R_\oplus) = 33.1^\circ$ is emphasized. Bottom panel; three values of the neutrino (continuous lines) and antineutrino (dotted lines) cross sections, as compared with the critical value of the cross section $\sigma_\star(\theta_{\rm N})$ related to e-folding absorption, as defined in the text.

4. High Energy Neutrino Telescopes

4.1. Operating Principles

The basic structure of a high-energy neutrino telescope is a matrix of light detectors inside a transparent medium. This medium, such as ice or water at great depths:

- offers a large volume of target nucleons for neutrino interactions;
- provides shielding against secondary particles produced by cosmic rays;
- allows the propagation of Cherenkov photons emitted by relativistic charged particles produced by the neutrino interaction.

The primary aim of these telescopes is the search for point sources and the characterization of the neutrino flux produced by diffuse/unresolved sources. While the idea in the former case is to stand out the atmospheric background in a specific direction of the sky, in the latter case the idea is to rely

fully on the study of the spectrum, in the hope that a cosmic component, harder than the one due to atmospheric neutrinos, can eventually become visible. This is illustrated in Figure 4 for the case of muon neutrinos.

Finally, a neutrino candidate can be characterized in *time* and *direction* of arrival, and it can be correlated with some temporal/spatial coincidence with an external triggers (such as that resulting from a γ-ray burst observation, from a gravitational wave event, or from other transients observed by space- or ground-based observations.) This last case is usually referred to as the *multimessenger strategy*. See Reference [52,53] for recent reviews. The *golden channel* for point-like neutrino source searches is represented by ν_μ's, where a (sub) degree pointing can be attained in the energy of interest.

Neutrinos are also characterized by their *flavor*, and each flavor and interaction mechanism induces different event topologies, as discussed in Section 5. The expected occurrence of neutrino oscillations give us a powerful manner to test the interpretation of the collected data (see Section 3.1).

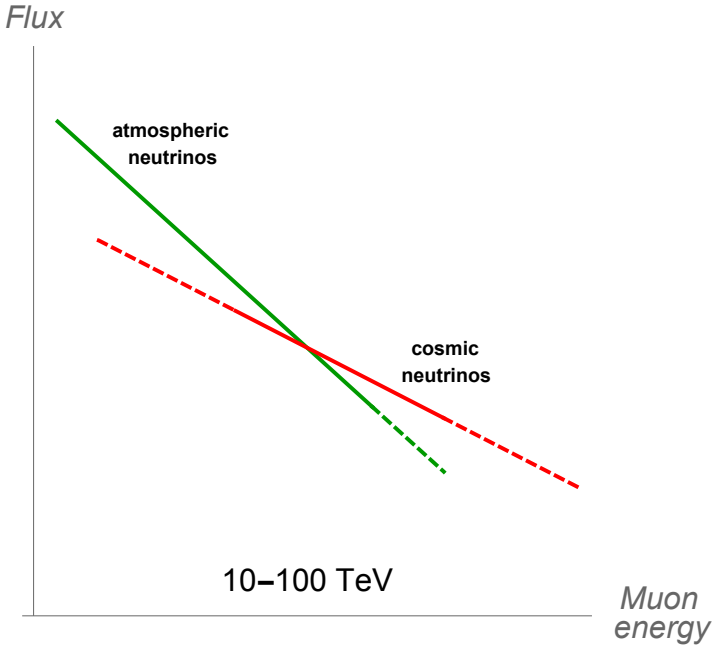


Figure 4. Schematic representation of how a new "hard" muon neutrino component of cosmic origin can stand out over the atmospheric neutrino at the highest energies, becoming observable. The energy regions where the uncertainties are larger are represented with dashed lines. For atmospheric neutrinos the uncertainty is due to the precise shape of the cosmic ray knee and the amount of prompt neutrinos; for cosmic neutrinos it is due to the production mechanism—moreover at low energies it is difficult to isolate them, while at high energies events are rare.

4.2. Detectors All Around the World

The activities for the construction of a neutrino telescope started in the early 1970s with a joint Russian-American tentative. Successively, the efforts of the two communities turned toward an experiment in a Russian lake with an iced surface and in the ice of South Pole. At the beginning of 1990's, European groups began the exploration of the Mediterranean Sea as a possible site for an underwater neutrino telescope. A detailed description of the experimental activities toward the realization of neutrino telescopes can be found in Reference [10].

4.2.1. IceCube

The IceCube experiment at the South Pole is, at present, the only running km^3-scale neutrino observatory. The instrumented detector volume is a cubic kilometer of highly transparent Antarctic ice instrumented with an array of 5160 Digital Optical Modules (DOMs). The IceCube array [54] is

composed of 86 strings instrumented each with 60 Digital Optical Modules (DOMs). Among them, 78 strings are arranged on a hexagonal grid with a spacing of 125 m, with a vertical separation of 17 m between each DOM. The eight remaining strings are deployed more compactly at the centre of the array, forming the DeepCore sub-detector [55]. A horizontal distance of 72 m separates the DeepCore strings with a vertical spacing of 7 m between each PMT.

The DOMs are spherical, pressure-resistant glass housings each containing a 25 cm diameter photomultiplier tube (PMT) plus electronics for waveform digitization, and vertically spaced 17 m from each other along each string. High quantum efficiency PMTs are used in a denser sub-array located in the center of the detector. This sub-array, called DeepCore, enhances the sensitivity to low energy neutrinos. Data acquisition with the complete configuration started in May 2011 [56].

4.2.2. ANTARES

In the sea, to minimize the noises induced by external agents, a telescope must be located far enough from continental shelf breaks and river estuaries. At the same time, the detector should be close to scientific and logistic infrastructures on shore. With such requirements, the Mediterranean Sea offers optimal conditions on a worldwide scale.

The ANTARES detector [57] was completed in 2008, after several years of site exploration and detector R&D. The detector is located at a depth of 2475 m in the Mediterranean Sea, 40 km from the French town of Toulon. It comprises a three-dimensional array of 885 optical modules (OMs) looking 45° downward and distributed along 12 vertical detection lines. An OM consists of a 10″ PMT housed in a pressure-resistant glass sphere together with its electronics [58]. The total length of each line is 450 m; these are kept taut by a buoy located at the top of the line. The instrumented volume corresponds to about 1/40 of that of IceCube, but due to the water properties, and the denser configuration of OMs, its sensitivity is relatively larger at energies below 100 TeV. In addition the Galactic center is below the horizon ∼70 % of the time.

4.2.3. KM3NeT

KM3NeT is a research infrastructure that will house the next generation neutrino telescope in the Mediterranean Sea [59]. KM3NeT will consists of two different structures.

The KM3NeT/ARCA telescope is in construction about 100 km off-shore Portopalo di Capo Passero (Sicily), at a depth of 3500 m. The DOM spacing along the DU is 36 m with an average distance among DUs of 90 m. ARCA will consists of two building blocks of 115 vertical detection units (DUs) anchored at a depth of about 3500 m. The telescope will have an instrumented volume slightly larger than that of IceCube. The main scientific objectives are the study of astrophysical potential neutrino sources, with particular attention for galactic ones [42]. The golden channel is the detection of long track muon produced in charged current ν_μ interactions. For this kind of events an angular resolution better than 0.1° and an energy resolution of 30% in log(Energy) are reached for neutrino energies greater than 10 TeV [59,60].

The KM3NeT/ORCA detector is located on the French site off-shore Toulon and at a depth of 2450 m. The main scientific objectives are the determination of the neutrino mass hierarchy and the searches for dark matter. The two KM3NeT facilities will also house instrumentation for Earth and Sea sciences for long-term and on-line monitoring of the deep-sea environment. The DOM spacing along the DU is 9 m and the average distance among the DUs is 23 m. It will consists of one building block, with an instrumented mass of 8 Mton.

Both KM3NeT structures will use the same DUs equipped with 18 optical modules, with each optical module comprising 31 small PMTs. The technical implementation and solutions of ARCA and ORCA are almost identical, apart from the different spacing between DOMs.

4.2.4. GVD

Finally, many years of experience with smaller neutrino telescope installations in Lake Baikal in Siberia, have led to the Baikal- Gigaton Volume Detector (GVD) project, aiming at a detector instrumenting a cubic-kilometer of water [61]. Baikal-GVD is formed by a three-dimensional lattice of optical modules, which consist of PMTs housed in transparent pressure spheres. They are arranged at vertical load-carrying cables to form strings. The telescope has a modular structure and consists of functionally independent clusters. Each cluster is a sub-array that comprises 8 strings. Each cluster is connected to the shore station by an individual electro-optical cable. The first cluster with reduced size was deployed and operated in 2015. In April 2016, this array has been upgraded to the baseline configuration of a GVD-cluster, which comprises 288 optical modules attached along 8 strings at depths from 750 m to 1275 m. In 2017–2019, four additional GVD-clusters were commissioned, increasing the total number of optical modules up to 1440 OMs. As part of phase 1 of the Baikal-GVD construction, an array of nine clusters will be deployed until 2021. GVD will primarily target neutrinos in the multi-TeV range. First results have recently been reported [62].

5. Topologies of the Events

In neutrino telescopes, one can distinguish between two *main* event classes—events with a long **track** due to a through-going muon (induced by ν_μ charged current (CC) interactions), and events with a **shower**, without the presence of a muon. The special case of ν_μ CC interactions inside the detector will contain a shower originating in the interaction vertex and an accompanying track as well.

A high-energy electron resulting from a CC ν_e interaction radiates a photon via bremsstrahlung after a few tens of cm of water/ice (the radiation length in water is $\sim$ 36 cm): this process leads to the development of an electromagnetic cascade (the *shower*). Showers are induced as well by neutral current interactions and by ν_τ CC interactions occurring inside the instrumented volume of the detector. Tau neutrino interactions can produce also a particular event topology, with events called in this review *double core*.

Neutrino and anti-neutrino reactions are not distinguishable; thus, no separation between particles and anti-particles can be made. A shower of particles is produced in proximity of the interaction vertex in all neutrino interactions. However, for CC ν_μ, often only the muon track is detected, as the path length of a muon in water exceeds that of a shower by more than 3 orders of magnitude for energies above 2 TeV. Therefore, such an event might very well be detected even if the interaction has taken place several km outside the instrumented volume, in the Earth's crust or in the surrounding transparent medium, provided that the muon traverses the detector. More in detail, the muon range R can be described in the continuous-energy-loss approximation as:

$$\frac{dR}{dE_\mu} = -\frac{1}{\alpha + \beta E_\mu} \text{ with } \begin{cases} \alpha \approx 2 \times 10^{-6} \ \frac{\text{TeV cm}^2}{\text{g}}, \\ \beta \approx 4 \times 10^{-6} \ \frac{\text{cm}^2}{\text{g}}. \end{cases} \tag{22}$$

The α coefficients describes the well-known fact that low energy muons *(minimum ionizing particles*, mip) loose about 2 MeV/cm in water, while the second coefficients β describes that the energy loss processes become 'catastrophic' at high energies. This implies the travel distance in water or ice ($\rho \simeq 1$ g cm^{-3}):

$$d(E_\mu, E_{\text{thr.}}) \approx D \times \log\left(\frac{1 + E_\mu/\varepsilon}{1 + E_{\text{thr.}}/\varepsilon}\right) \text{ with } \begin{cases} D = \dfrac{1}{\rho \cdot \beta} \approx 2 \text{ km} \\ \varepsilon = \dfrac{\alpha}{\beta} \approx 0.5 \text{ TeV}. \end{cases} \tag{23}$$

The properties of showers (total visible energy, a rough estimate of the neutrino direction) are obtained if the interaction occurs inside (or very close to) the instrumented volume. Figure 5 shows a sketch of neutrino interactions giving the two different types of events.

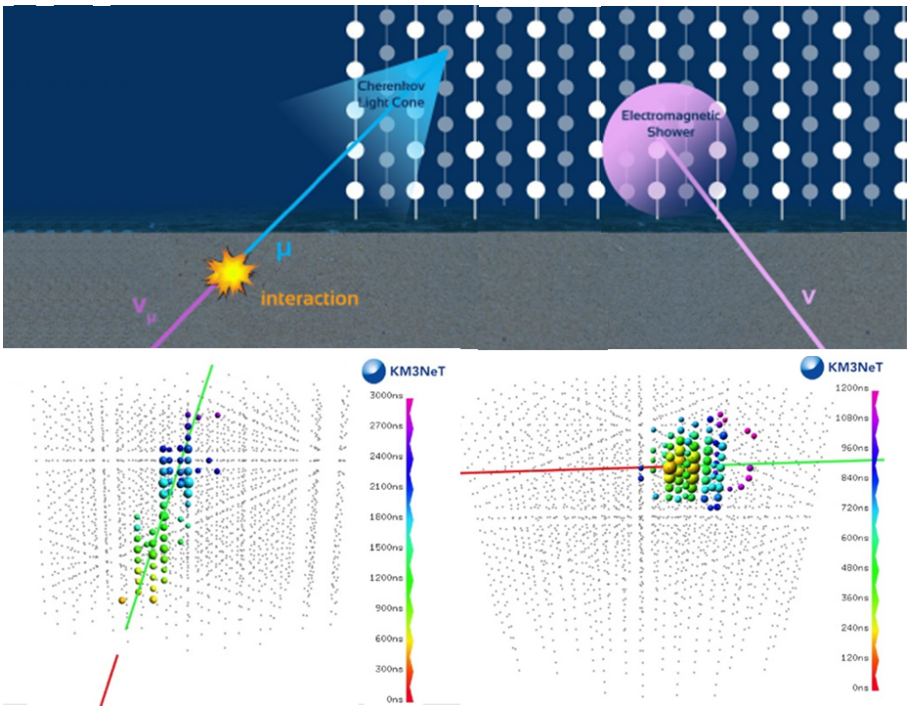


Figure 5. Neutrino interactions give two different types of events: ν_μ charged current (CC) interaction that produces a muon (left) and ν_e CC interaction that produces an electron inducing an electromagnetic cascade (shower). Neutral current (NC) interactions also produce showers. In this sketch, provided by the KM3NeT Collaboration, each point represents an optical module (OM), spaced about 100 m from each other. In gray are the OMs not interested by optical photons (mainly from the Cherenkov effect) produced by the event. The colors show the temporal sequence of the hit OMs—the red color indicates the beginning of the event.

5.1. Passing-Events

Passing-events are due to tracks induced by ν_μ and $\bar{\nu}_\mu$ CC interactions around the detector and passing through the detector. The same signal is called (depending on the experiment) also through-going muons, up-going muons, passing muons, tracks, and so forth emphasizing a feature or another one. (As recalled above, there is also the possibility of track events that start inside the detector.)

The angular precision for passing-events depends on the muon energy and detection medium. Deep ice is more transparent than seawater. Thus, the same instrumented volume of ice corresponds to a larger effective volume than in seawater. On the other hand, the effective scattering length for ice is smaller than water. This is a cause of a larger degradation of the angular resolution of detected neutrino-induced muons in ice with respect to water. Passing-events are better reconstructed in seawater than in ice. Refer to Reference [18] for a detailed discussion of differences between water and ice properties. The typical angular resolution of tracks in ice, $\delta\theta_{\text{passing}} \sim 0.5 - 1^\circ$, while it is foreseen to reach 0.1° in the KMeNeT detector.

Passing-events are mostly selected from the direction of the Sky below the detector, in order to keep under control the background of atmospheric muons. Therefore, the neutrinos that have to cross a large fraction of the Earth, above few 100 of TeV, are subject to absorption (Section 3.2); the optimal region of observation is therefore a crown of azimuthal directions, just below the horizon of the detector.

5.2. Contained Events

The first operating km^3-class telescope, IceCube, has demonstrated that also events partially or fully contained in the detector can be used to observe high-energy cosmic neutrinos.

The method rely on the request that the interaction point, and possibly the whole event, is located into the instrumented volume. In this manner, the background can be suppressed, and this is even more effective for electron type events, that are less abundant among atmospheric neutrinos. The ratio of the through-going events with respect contained ones is roughly given by

$$\frac{N_{\text{throug.}}}{N_{\text{contained}}} \sim \frac{\text{area} \times D}{\text{volume}} \tag{24}$$

where a detector with typical dimension L has an area $\sim L^2$ for muon detection and a volume L^3 for contained event detection. The scale distance D is defined in Equation (23). The ratio is just $\sim D/L$ and this is not small as long as the detector has physical dimension $L \sim D$ namely, kilometer size, just what has been attained by IceCube.

This method allows the telescope to observe also events coming from *above* the detector, differently from the previous method. However, the risk of background contamination from atmospheric muons does exist, especially at the lowest energies. For zenith angles $\theta < 70^\circ$ and $E_\nu > 100$ TeV the atmospheric muon self-veto (Section 6.2) can help to suppress the atmospheric neutrino background.

5.3. Double Core Events

The presence of ν_τ would be an unequivocal signature of a cosmic neutrino. The direct production in cosmic ray collision is very suppressed. High-energy atmospheric neutrinos do not have enough time to undergo flavor transformation. Thus, with high confidence, ν_τ are produced through three flavor oscillations over cosmic scale distances (Section 3.1).

The identification of a ν_τ relies on the extrapolation on macroscopic scales of the principle used by OPERA, namely, the displacement between the point where the tau lepton is produced (by a CC ν_τ interaction) and the point where the charged tau decays. There are two different implementations of this principle. In the first one, different regions of a neutrino telescope (namely, different strings or set of phototubes) see the two interaction vertexes. In the second one, using the fast time response of each individual phototube, the experiment is able to distinguish light emission occurred in two successive processes (the ν_τ interaction, the τ decay). These two principles are known as *double bang* [63] and *double pulse* [64] respectively—and collectively are called *double core events* in the present review paper.

5.4. Glashow Resonance

An exciting possibility is the observation of events caused by $\bar{\nu}_e$ interacting with atomic electrons, and producing an on-shell W boson via $\bar{\nu}_e + e \to W$. The cases when the W decay in a pair of quarks yields the whole energy of the initial neutrino, amounting to

$$E_{\text{Glashow}} = \frac{m_W^2}{2m_e} = 6.3 \text{ PeV} \tag{25}$$

This process yields a conventional observable shower; however, due to the large cross-section, this would incredibly enhance the opportunity to observe PeV-energy $\bar{\nu}_e$. An events at a such energy, yet unseen, is called *Glashow resonance* [65].

Seeing events due to Glashow resonance would be an excellent way to probe of the extension of the cosmic neutrinos spectrum at high energies, and in the long run, also a test of the type of neutrino source (whether pp or $p\gamma$). See Reference [66] for an updated, quantitative discussion.

5.5. Effective Areas

For each event topology, the calculation of the expected number of neutrino signals N_i, given a flux of neutrinos of type ℓ, is usually performed by means of *effective areas* $A_{\ell \to i}$. If the flux is constant in time and the observation time is T, it is possible to write symbolically:

$$N_i = 4\pi T \int dE_\nu \; A_{\ell \to i}(E_\nu) \; \Phi_\ell \tag{26}$$

The effective area incorporates the neutrino cross section, the number of target particles in the detector, the angular and the energy response, the detector inefficiencies, the cuts implemented in the analysis. Usually, it is a growing function of the energy of the incoming neutrino. In the IceCube detector the effective areas for the main classes of events, the passing (muon) events and the contained events, are about some tens of m^2 in the relevant energies. The effective area for contained events at high-energies increases mostly because of the cross section growth with neutrino energy, $\sigma \sim E_\nu^{0.3-0.4}$; see Reference [67] for a useful and accurate discussion.

6. Background Processes

The cosmic neutrino sky as seen on Earth is not background free, due to the presence of the atmospheric neutrinos and secondary atmospheric muons.

6.1. Atmospheric Neutrinos

In the region of energy where atmospheric neutrino oscillations have been discovered, $E_\nu \sim$ GeV, the spectrum of the neutrinos is distributed as $E_\nu^{-\alpha}$ with $\alpha \sim 2.7$. In fact, due to the mentioned property of *scaling* of the hadron-hadron interactions, atmospheric neutrinos have (approximatively) the same power-law index of the primary cosmic rays at the corresponding energies. Neutrino telescopes have been able to measure the flux and energy spectrum of atmospheric ν_μ [68,69] and atmospheric ν_e [70].

This behavior changes at the higher energies of interest for the search of cosmic neutrinos, because most secondary muons in Equation (3), will touch ground before decaying. This reduces the number of atmospheric ν_μ and depletes electron neutrinos: indeed, the electron/muon neutrino fraction decreases from 1/2 to 1/30, because the muon is not allowed to decay freely. Pions of similar energy travel 100 times less before decaying; however, they have a nuclear interaction cross section of the order of $\sigma_\pi \sim \pi \times \text{fm}^2$ with nucleons, which implies an interaction length $m_n/(\sigma_\pi \times \rho_{\text{air}})$ of comparable size for a density of $\rho_{\text{air}} \sim 10^{-3}$ g/cm^3. For this reason, spectrum of atmospheric neutrinos from pion interactions becomes steeper, $E_\nu^{-\alpha}$ with $\alpha \sim 3.7$, since only a fraction of pions is free to decay before interacting. This is the behavior of the atmospheric component shown in Figure 4.

It is important to recall that at some 10–100 TeV one expects the onset of a new component (to date unobserved) due to the production of charmed mesons, that, having a very short lifetime, decay immediately after production leading to a spectrum as $E_\nu^{-\alpha}$ with $\alpha \sim 2.7$ and with an approximately equal amount of electron and muon neutrinos. A very interesting possibility to emphasize and possibly observe the prompt contribution is to identify a clean sample of *non-muonic neutrinos* in the region of 10-few 10 of TeV, as discussed in Reference [48]. In this paper one finds a description of the model of atmospheric neutrinos, of the one of cosmic neutrinos (based on the hypothesis of pp-collisions and upgraded thanks to IceCube through-going muon data), and an assessment of their uncertainties. For an illustration of the principle, see Figure 6.

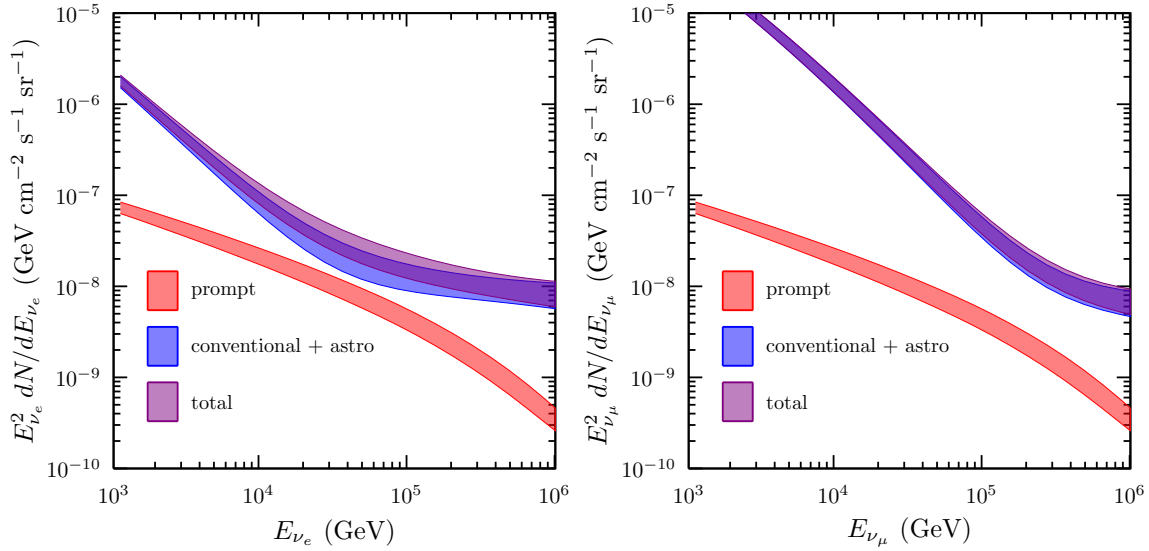


Figure 6. The expected electron (left panel) and muon neutrino (right) flux components in the energy range from 1 TeV to 1 PeV. Prompt neutrinos are shown separately and summed with all other components. From Reference [48].

6.2. Atmospheric Muons

Atmospheric muons can penetrate the atmosphere and up to several kilometers of ice/water, and they represent the bulk of reconstructed background events in any large volume neutrino detector [71–73]. Neutrino detectors must be located deep under a large amount of shielding in order to reduce the background. The flux of down-going atmospheric muons exceeds the flux induced by atmospheric neutrino interactions by many orders of magnitude, decreasing with increasing detector depth, as shown in Figure 7.

Atmospheric muons can be used for a real-time monitoring of the detector status and for detector calibration [74]. However, they represent a major background source: downward-going particles wrongly reconstructed as upward-going and simultaneous muons produced by different cosmic ray primaries could mimic high-energy neutrino interactions, see [75] for a discussion.

In general, atmospheric neutrinos are indistinguishable from astrophysical neutrinos. The presence of a muon can help to classify a contained interaction as due to atmospheric ν_μ instead of a cosmic ν_μ. This occurs when neutrino energy is sufficiently high and the zenith angle sufficiently small that the muon produced in the same decay as the neutrino has a high probability to reach the detector [76,77]. In this case, the atmospheric neutrino provides its own self-veto. In general, the atmospheric neutrino passing rate can be evaluated with simulations by including other high-energy muons produced in the same cosmic-ray shower as the neutrino. In this way, the method can be extended to ν_e's [78]. In practice, the passing rate is significantly reduced for zenith angles $\theta < 70^\circ$ and $E_\nu > 100$ TeV. This method was used first by the IceCube collaboration to select the high energy starting events (Section 5.2).

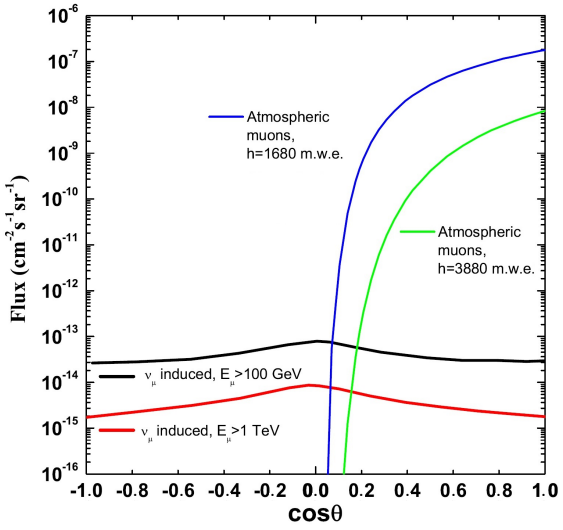


Figure 7. Flux as a function of the cosine of the *zenith angle* θ of: (i) atmospheric muons for two different depths; (ii) muons induced by CC interactions of atmospheric ν_μ, for two different muon energy thresholds E_μ. Upgoing (down-going) events have $\cos\theta < 0$ (>0) [75].

7. The Observational Status of High-Energy Neutrinos Astronomy

The IceCube experiment has observed neutrinos of astrophysical origin in different ways [79,80]—first with the *High Energy Starting Event (HESE)* sample; then with passing events; finally with a coincidence with electromagnetic signals.

7.1. Contained Events

The first detailed observation of an excess of high-energy astrophysical neutrinos over the expected background has been reported by IceCube using data collected from May 2010 to May 2012 and with 662 days live time [81]. This sample is continuously updated, and as of this writing (after ICRC 2019), results up to early 2018 are available for a total live time of 2635 days of live time. The high-energy neutrino candidates have been selected with the requirement that the interaction vertex is contained within the instrumented ice volume, without any signal on the PMTs located on the top or sides of the detector. In such a way, the edges of IceCube are used as a veto for down-going atmospheric muons and atmospheric neutrinos, Section 6.2.

The deposited energy E_{dep} in the detector is derived from the number of photoelectrons (p.e.) in the optical modules and, in turns, the true energy E_ν of the neutrino is estimated with the help of Monte Carlo simulation techniques. An event with 6000 p.e. corresponds to a deposited energy of $\sim$30 TeV.

Figure 8 shows the distribution of the deposited energy (left plot) and of the cos(declination) (right plot) for HESE in the 7.5-year sample. The additional contribution in the data sample with respect to the background corresponds to a diffuse astrophysical signal, with topologies compatible with neutrino flavor ratio $\nu_e : \nu_\mu : \nu_\tau \sim 1 : 1 : 1$, as expected for a cosmic signal [82]. The best fit to the data above 60 TeV [83] yields, for all neutrino flavors (6ν means the sum over neutrino and antineutrinos of all flavors),

$$\frac{d\Phi_{6\nu}}{dE} = (6.45^{+1.46}_{-0.46}) \cdot 10^{-18} \left(\frac{E}{100\ \text{TeV}}\right)^{-(2.89\pm0.2)} \text{GeV}^{-1}\ \text{cm}^{-2}\ \text{s}^{-1}\ \text{sr}^{-1}\ . \quad (27)$$

Most of the signal originates primarily from the Southern hemisphere, where neutrinos with $E_\nu \gg 100$ TeV are not absorbed by Earth. The poor angular resolution ($\sim$15°) of showering events prevents the possibility of accurate localization in the sky of the parent neutrino's direction. To identify

any bright neutrino sources in the data, the usual maximum-likelihood clustering search has been used, as well as searches for directional correlations with TeV γ-ray sources. No hypothesis test has yielded statistically significant evidence of clustering or correlations.

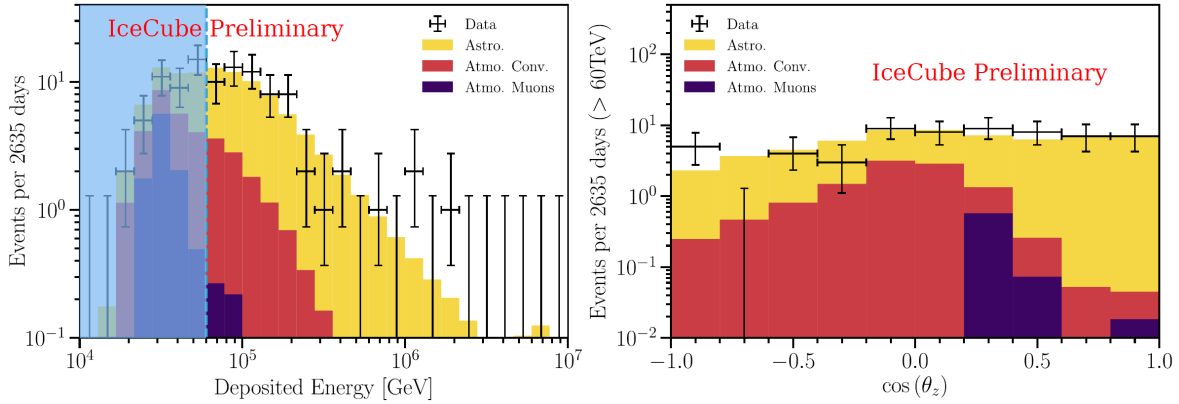


Figure 8. Deposited energies E_{dep} (left panel) and arrival directions (right panel) of observed IceCube HESE (crosses), compared with predictions. The sample refers to 7.5 years of data. The best-fit expectation is shown as a stacked histogram with each color specifying a flux component—astrophysical (golden), conventional atmospheric (red), and penetrating muons (purple); the best fit prompt normalization is zero and is not shown. Events below 60 TeV (light blue vertical line) are not included in the fit, but one sees good data-MC agreement extending into this energy range. From the arXiv version of [83].

7.2. The Passing Muons

A second IceCube sample that evidences a diffuse presence of cosmic neutrinos corresponds to CC upgoing muon neutrino events [84,85]. The field of view for these events is restricted to the Northern hemisphere. This analysis has recently been extended with data collected up to December 2018, equivalent to 10 y of live time [86]. This last sample contains ∼650,000 muon neutrino candidates.

For these events, the reconstructed energy E^i_{rec} of each individual neutrino i is a poor proxy of the true neutrino energy, E_ν. Thus, the reconstructed neutrino energy is used to produce a response matrix $P(E^i_{rec}; E_\nu)$, which must be inverted to produce the posterior probability density function $P(E_\nu; E^i_{rec})$ [85]. Figure 9 shows the distribution of the observable energy for the eight-year sample. A clear excess above $\sim$ 100 TeV is visible and is not compatible with the atmospheric background expectation.

When the atmospheric neutrino background is removed, the best fit to the full data-set results in an astrophysical power-law flux for one neutrino flavor (i.e., $\nu_\mu + \bar{\nu}_\mu$) [86]:

$$\frac{d\Phi_{2\nu}}{dE} = (1.41^{+0.25}_{-0.24}) \cdot 10^{-18} \left(\frac{E}{100\ \text{TeV}}\right)^{-(2.28\pm0.09)} \text{GeV}^{-1}\ \text{cm}^{-2}\ \text{s}^{-1}\ \text{sr}^{-1}\ . \quad (28)$$

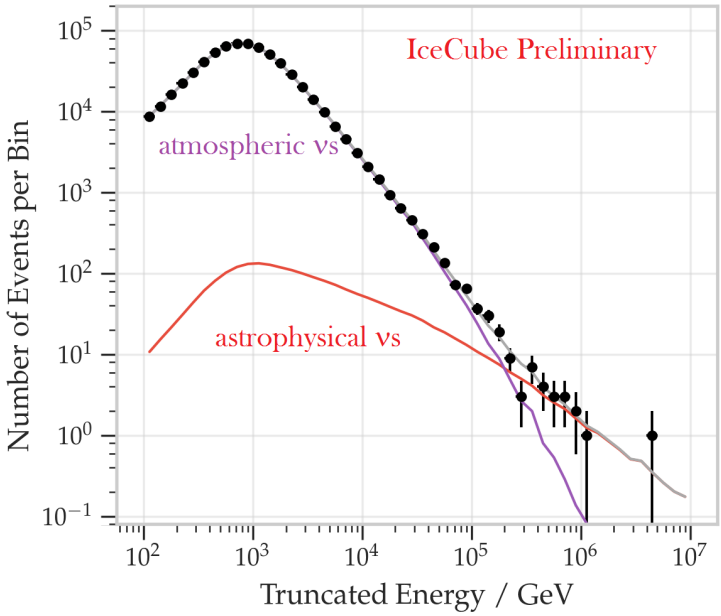


Figure 9. Unfolded ν_μ event distribution from the passing muon sample in IceCube. The data (crosses) are compared to the best-fit fluxes for atmospheric and astrophysical neutrinos. From the arXiv version of [86].

7.3. The Observation from TXS 0506 + 056

On 22 September 2017 (the month following the first observation of the coalescence of the two neutron stars with gravitational waves), the IceCube collaboration detected a track event induced by a ∼300 TeV ν_μ. The detection generated an automatic alert that caused related searches from the direction of the event by many experiments. The Fermi-LAT satellite telescope reported that the direction of the neutrino was coincident with a known gamma-ray source, the active galaxy known as TXS 0506 + 056 (object classified as a blazar), that was in a particularly active state at the time of the neutrino detection. In addition, the MAGIC gamma ray telescope (located at the Canary Islands) also observed a significant photon flux of energies up to 400 GeV from the direction of the blazar; the study of the astronomical object was completed by observations at other wavelengths: radio, optical and X-ray. These observations are compatible with the position of a known blazar at redshift $z = 0.3365 \pm 0.0010$ [87]. Neutrino correlation with the registered activity of TXS 0506 + 056 was classified as statistically significant at the level of 3 standard deviations [88].

Triggered by this association, the IceCube collaboration analyzed their data (corresponding to 9.5 years) to search for a neutrino emission in excess to the background from the direction of the blazar. An excess was found in the period between September 2014 and March 2015, with statistical significance estimated at 3.5 standard deviations, independent of and before the 2017 flaring episode [89].

The reconstructed direction of the IceCube neutrino corresponded, at the location of the ANTARES detector, to a direction 14.2° below the horizon. A possible neutrino candidate would thus be detected as an up-going event. A time-integrated study performed by the collaboration over a period from 2007 to 2017 fits 1.03 signal events, which corresponds to a probability that the background simulates this signal of 3.4% (not considering trial factors) [90].

7.4. Studies of the Galactic Region

Due to their relative proximity, the possibility of studying Galactic sources is particularly intriguing.

The ANTARES detector in the Northern hemisphere can measure *upgoing events*, exploiting, with respect to IceCube, its complementing field-of-view, exposure, and lower energy threshold [91]. In particular, ANTARES is sensitive at a level compatible with the larger IceCube detector to possible

sources located in the Galactic plane. Although a sizable neutrino flux from individual sources is expected to be observable only with a km^3-scale detector (see Figure 2), detailed searches for point-like and extended sources of cosmic neutrinos from the Galactic region have recently been performed using data collected by the ANTARES and IceCube neutrino telescopes [92]. They combined all the track-like and shower-like events pointing in the direction of the Southern Sky included in a previous nine-year ANTARES point-source analysis, with the through-going track-like events used in a seven-year IceCube point-source search. The advantageous field of view of ANTARES and the large size of IceCube are exploited to improve the sensitivity in the Southern Sky by a factor of $\sim$2 compared to both individual analyses. A special focus was given to the region around the Galactic Centre, whereby a dedicated search at the location of SgrA* was performed, and to the location of the supernova remnant RXJ 1713.7-3946. No significant evidence for cosmic neutrino sources was found; upper limits on the flux are presented in Figure 10.

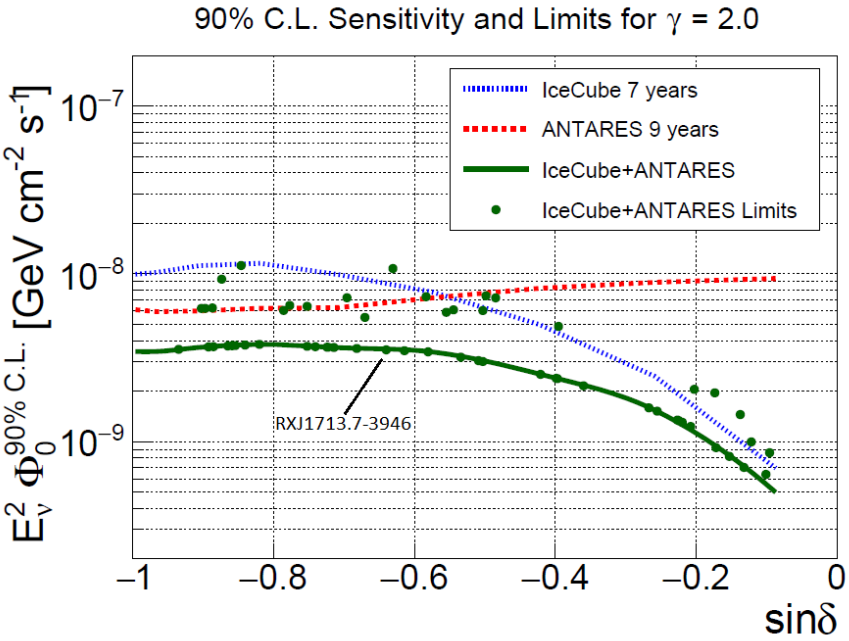


Figure 10. Upper limits at 90% C.L. on the $\nu_\mu + \bar{\nu}_\mu$ neutrino flux normalization from 57 neutrino candidate sources (green dots) studied by the ANTARES and IceCube collaborations, as a function of the source declination [92]. Such kind of plots depends strongly on the assumption of the neutrino energy spectrum and on the differential sensitivity of the detectors. The present plot is computed assuming an unbroken neutrino spectrum, with spectral index $\gamma = 2.0$. For this spectrum, most of signal is due to neutrinos with $E_\nu > 10$ TeV. The green line indicates the sensitivity of the combined analysis. The dashed curves indicate the sensitivities for the IceCube (blue) and ANTARES (red) individual analyses. Referring to Figure 2, the limit corresponding to the SNR RXJ1713.7-3946 is indicated (when comparing the two plots, remember that the y-axis of this figure must be multiplied by 10^{-3} to have the same units).

In this figure, the upper limit corresponding to the SNR RXJ1713.7-3946 is highlighted in order compare it with the predictions reported in Figure 2. The predicted flux at $E_\nu > 10$ TeV is of the order of few$\times 10^{-9}$ GeV cm^{-2} s^{-1}, which is still slightly below the combined ANTARES (9 years) and IceCube (7 years) sensitivities.

In addition to individual sources, the existence of a diffuse Galactic neutrino production is expected from cosmic-ray interactions with Galactic gas and radiation fields. These interactions are also the dominant production mechanism of the diffuse high-energy γ-rays in the Galactic plane,

which have been measured by the Fermi-LAT. Different models propagating charged cosmic rays diffusively in the interstellar medium producing γ-rays and neutrinos via interactions with the interstellar radiation field and interstellar gas have been developed. The ANTARES and IceCube combined their analyses to test [93] a specific neutrino production model (Figure 11). As a result, their estimate yields a non-zero diffuse Galactic neutrino flux for a p-value of 29% for the most conservative model.

The result of this analysis limits the total flux contribution of diffuse Galactic neutrino emission to the total astrophysical signal reported by IceCube above 60 TeV to be less than 10%.

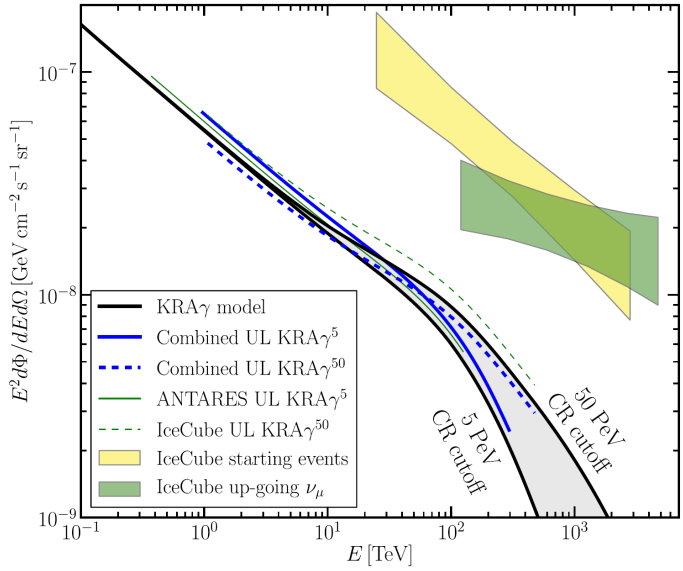


Figure 11. Combined upper limits from ANTARES and IceCube (at 90% confidence level, blue lines) on the three-flavor neutrino flux of the model of Galactic cosmic ray propagation (the black lines shows two values of the knee position). The boxes represent the diffuse astrophysical neutrino fluxes measured by IceCube using an isotropic flux template with starting events (yellow) and upgoing tracks (green) [93].

8. What Are the Main Sources of Cosmic Neutrinos?

The diffuse extraterrestrial flux of high-energy neutrinos, highlighted by IceCube and discussed above, has characteristics that suggest significant extragalactic contributions. This seems to be confirmed by the observation concerning TXS 0506 + 056. In spite of that particular association, the individual sources of IceCube neutrino events remain unidentified [94].

At present, the IceCube and ANTARES collaborations manage a series of alert and follow-up programs, which react in real time to events due to neutrino interactions classified as particularly interesting. In this case, a short message is automatically sent to the Gamma-ray burst Coordinates Network (the GCN network) [95], which activates the radio, optical, X-ray and gamma telescopes. Conversely, particular transient phenomena observed with other probes can be immediately studied with the network of neutrino telescopes.

Although we do not have yet a clear theoretical idea on which the sources of cosmic neutrinos are and how intense they are, there are several ideas on the subject. In this section, largely based on Reference [23], we discuss a few cases when cosmic neutrinos are directly connected to the (sources of the) cosmic rays.

8.1. Cosmic Rays and Cosmic Neutrinos

Consider an astrophysical site where cosmic rays are produced and confined for some time, and suppose that the same region also contains a 'thin' target— much more diffuse than in Earth's atmosphere. As described in Section 2.1, we might imagine that this site will be particularly brilliant in neutrinos and γ-rays, and that the shape of these secondary particles will reflect the production spectra of cosmic rays. The cosmic ray spectrum in the source is unknown *a priori*, however, general theoretical arguments are in support of the idea that the spectrum behaves as $\sim E_{\rm CR}^{-2}$, both for γ-rays and for neutrinos. (1) First, such a spectrum is expected for primary cosmic rays in the Fermi acceleration mechanism. (2) Second, if the target for the cosmic ray collisions is composed by protons or other nuclei, but–differently from the atmosphere–the target layer is thin and there is no significant absorption of the mesons, the spectra of the secondary particles reflect closely the shape of the primary cosmic ray spectrum. (3) Third, it is not plausible that neutrinos suffer absorption in the source - while for gamma rays, this is possible. In these conditions, the spectrum of the secondary neutrinos (and possibly of the associated γ-rays) till some maximum energy, is expected to be distributed as $\Phi_\nu \propto E_\nu^{-2}$. This spectrum would stand out over the atmospheric neutrino background at sufficiently high energies - see again Figure 4.

8.2. Extragalactic Sources

Nowadays, extragalactic sources are believed to give the dominant contribution to the high energy neutrino flux. Assuming that the highest energy cosmic rays that we observe on Earth are typical of the entire cosmos and are of extragalactic origin, we estimate that they have an energy density of $\rho_{\rm uhecr} = 3 \times 10^{-19}$ erg/cm^3 above 1 EeV. Considering the typical evolution time of $T_H = 10$ billion years, the corresponding energy losses of the universe are $W = \rho_{\rm uhecr}/T_H = 9 \times 10^{44}\,{\rm erg}/({\rm Mpc}^3\,{\rm yr})$. This cosmic ray population will be in equilibrium if, in the reference volume of 1 Gpc^3, there is a population of 900 γ-ray bursts and each one injects suddenly 10^{51} erg in cosmic rays; an alternative would be that there is a population of 150 active galactic nuclei, and each one radiates continuously 2×10^{44} erg/s. Interestingly, in both cases, the number of sources is reasonable and the presumed amount of energy emitted in cosmic rays corresponds to the visible electromagnetic output.

There are many potential astrophysical sources of high energy neutrinos and below we provide a brief summary of the most significant ones, examining AGNs, blazars, starburst galaxies and Gamma-Ray Bursts (GRBs).

8.2.1. Active Galactic Nuclei

An active galactic nucleus (AGN) is a compact region at the center of a galaxy whose luminosity is much higher than the normal one over some portion of the electromagnetic spectrum, with characteristics indicating that the excess luminosity is not produced by stars. This excess (in the non-stellar emission) has been observed in the radio, microwaves, infrared, optical, ultra-violet, X-ray and gamma ray wavebands. The radiation from an AGN is believed to be a result of accretion of matter by a supermassive black hole at the center of the host galaxy [96]. The central engine can accelerate protons up to very high energies, while the accretion disc is an emitter of hot thermal radiation, which gives prominent feature in the observed AGN spectra, usually refereed to as a "Big Blue Bump". Accelerated particles move along two jets perpendicular to the accretion disc and crossing this radiation field. AGNs are characterized by a strong positive cosmic evolution, meaning that these objects were much more abundant in the past.

AGN's are considered potential sites for high energy neutrino production since 30 years [97–99]. High energy neutrino appear in charged pion decays created in proton-γ interactions, Equation (5), due to the collision between protons and the "blue bump" photons. Protons can be accelerated up to $\sim$EeV energies and absorbed in the radiation field contained in the disk, that has a temperature of the order of 10 TeV and a black hole mass of $\sim 10^8 M_\odot$. Therefore the resulting neutrino flux is

expected to be relevant in the sub-PeV and in the PeV region. One clarification is needed: as explained in Section 2.2, neutrinos from pp or $p\gamma$ interactions takes 5% of the primary proton energy. However, during the propagation, neutrinos looses energy adiabatically, reaching the Earth with an energy equal to $(E_p/20)/(1+z)$, where E_p is the primary proton energy. Since the distribution of AGNs is strongly positive, the larger contribution to the neutrino emission is provided by sources having redshift between $z = 1$ and $z = 2$. It means that most of high energy neutrinos reaching Earth, will have an energy $\sim$50 times lower than the energy of the primary proton.

Nowadays it is not possible to exclude (or confirm) the AGNs as potential sources of a part of the IceCube signal. The increasing of the statistics can help in this game, although it is hard to constrain certain class of abundant sources (such as low luminosity AGNs).

8.2.2. Blazars

Blazars are AGNs with the emitted jet pointing toward the Earth. They are divided in two classes: BL Lacertae (BL Lac) and Flat Spectrum Radio Quasar (FSRQ). FSRQs are characterized by the presence of a broad line region and by emission lines in the optical spectrum, while BL Lacs are characterized by featureless optical spectra (i.e., lacking strong emission/absorption lines). A complete review of the processes occurring in blazars is provided in Reference [100].

The Fermi-LAT satellite proved that the blazars are the brightest extragalactic sources above 10 GeV. Many more of these blazars are not visible as point sources, being too faint and/or too far from us. They contribute to the unresolved γ-ray radiation, again observed by Fermi-LAT. The sum of resolved and unresolved blazars almost saturates the observed diffuse emission, providing $\sim$ 80% of the Extragalactic Gamma-ray Background (EGB) above 100 GeV [101], with a margin of uncertainty of some ten percents, that should be attributed to other sources.

Since blazars dominate the γ emission, it is natural to consider them also as high energy neutrino emitters [102–107]. Particularly, FSRQs are expected to be very efficient in the neutrino production, due to the interaction that can occur in the broad line region. Moreover, as discussed in Section 7.3, up to now the only confirmed sources of one high energy neutrino is a blazar.

However FSRQs (and high luminosity blazars in general) are not abundant in the universe. To have an idea, blazars having a gamma-ray luminosity larger than $L_\gamma = 10^{45}$ erg/s have a local density of 10 sources per Gpc^{-3}. For these reasons if high luminosity blazars were the sources, at least two or more neutrinos from the one FSRQ would be expected. This is not observed in the present neutrino data, meaning that blazars cannot contribute more than 20% to the observed high energy neutrino flux [107]. It is important to remark that this result does not say anything on the possible contribution of blazars at higher energies. For example, blazars may dominate the emission in the multi PeV-EeV energy range, but nowadays we do not have the technology to observe such a flux, since the flux decreases with the increasing of the energy in any plausible production mechanism.

In Figure 12 the problem due to the absence of multiplets is clearly shown. A multiplet is defined as two or more events from the same source (within the angular resolution of track-like events, order of 1°) during the time window in which data have been collected by IceCube. Up to now no multiplets are present in the IceCube measurements. The purple region represents the local power density required to match the flux measured by IceCube. The blue regions denote the parameter space excluded from the absence of multiplets in the neutrino data. We see in the left panel that sources that are brilliant but rare (like FSRQs) are excluded by the present measurements.

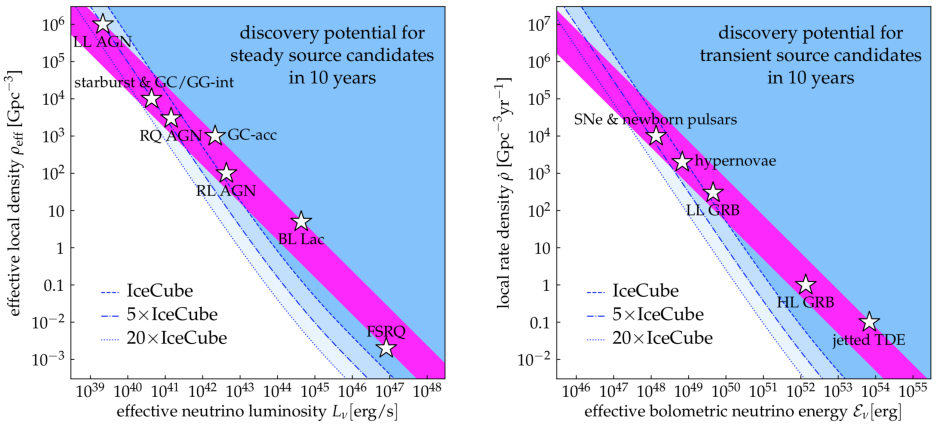


Figure 12. Figure from Reference [108]. The purple bands show the power required to interpret the flux of astrophysical neutrinos detected by IceCube (steady sources on the left, transient sources on the right). The blue regions show the parameter space excluded by the absence of multiplets in the neutrino data (i.e., two or more events from the same source). Sources that are abundant and faint (top left of the panels) are favorite by the data.

8.2.3. Starburst Galaxy

The starburst galaxies are a subset of star forming galaxies (SFGs) that undergo an episode of vigorous star formation in their central regions. The gas density is much higher than what is observed in quiescent galaxies and for this reason the pp interaction is a plausible mechanism to produce high energy neutrinos. Particularly the star formation rate can be 10–100 times higher that the one of Milky Way. Diffusion in starburst galaxies might also become weaker due to strong magnetic turbulence, while advective processes might be enhanced. Since the losses by inelastic collisions and advection are nearly independent of energy, the hadronic emission of starburst is expected to follow more closely the injected cosmic ray nucleon spectrum, $E^{-\alpha}$, with $\alpha \simeq 2.15$ [109–111].

The nearest starburst galaxies are M82 and NGC 253, both at a distance of 3.5 Mpc. These galaxies exhibit relatively hard γ-ray spectrum in the GeV to TeV energy range, with a spectral index between 2.1 and 2.3. Especially the γ-ray spectrum of NGC 253 has been well measured by both Fermi-LAT and H.E.S.S. experiments. Due to the harder emission spectrum and a higher pion production efficiency, the starburst subset is predicted to dominate the total diffuse γ-ray emission of SFGs beyond a few GeV, while above 10 GeV the contribution of blazars becomes dominant. Provided that the cosmic ray accelerators in starburst galaxies are capable of reaching energies of $\sim$ 10 PeV per nucleon, the hadronic emission can also contribute significantly to the diffuse neutrino emission at PeV energies. However a problem related to the Multimessenger connections between neutrinos and γ-rays comes out in this scenario.

Indeed, in proton-proton (pp) interaction an about equal amount of π^+, π^0 and π^- is produced. Taking into account also the sub-dominant contribution of kaons, the emitted all flavor neutrino flux is almost equal to the emitted γ-ray flux. After the propagation the two fluxes become very different, because neutrinos lose energy only adiabatically while γ-rays at TeV scale interact with the Extragalactic Background Light (EBL) and the energy is redistributed in the 1–100 GeV energy range approximately with a E^{-2} spectrum. However, it is possible to connect the measured neutrino flux with the associated expected γ-ray, taking into account the effect of the propagation. This has been done in two works, finding different results. If one relies on the IceCube HESE sample (Section 7.1), the measured neutrino spectrum is very soft and the associated gamma-ray flux would be too high [112], overshooting the possible contribution to the extragalactic background expected from Starburst Galaxies ($\sim$ 20% above 50 GeV). Following this result, the contribution of starburst galaxies would be at level of 10% (see left panel of Figure 13). However if one relies on the through-going muon flux, starburst galaxies are still perfectly compatible with astrophysical neutrinos [113] (see right

panel of Figure 13). Moreover the absence of multiplets in neutrino data suggests that high energy neutrinos are produced by abundant and faint sources; following this argument, starburst galaxies would be an ideal candidate. Future detections are required to improve the knowledge of the origin of astrophysical neutrinos.

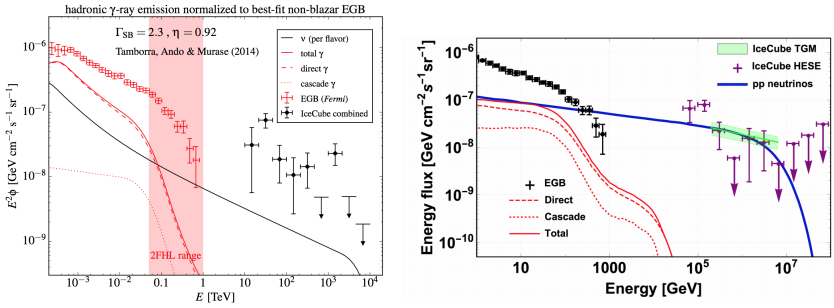


Figure 13. Multimessenger comparison between the flux of astrophysical neutrinos and the associated flux of γ-rays. In the left panel, High Energy Starting Events for the neutrino flux are used (figure from Reference [112]). In the right panel through-going muons are used (figure from Reference [113]).

9. Discussion and Prospects

The present status of neutrino astrophysics is extremely exciting, with very intriguing perspectives. The first general remark is that the total number of cosmic neutrinos is small. Due to the not null background from atmospheric neutrinos, usually each neutrino candidate is tagged with an *event signalness*. This is a parameter (used firstly by the IceCube collaboration to classify their neutrino candidates) defined as the ratio of the astrophysical expectation over the sum of the atmospheric and astrophysical expectations for a given energy proxy and a specific neutrino flux. Events with high signalness ($>$0.5) are usually high-energy events. The signalness is dependent on assumptions, for example, on the cosmic neutrino flux that is derived from data itself. The number of events with high signalness in IceCube are about 3 passing-events above 200 TeV a year (where 1 of them on average should be due to background) and about twice as many HESE events with deposited energy $>$ 60 TeV. The features of the energy flux for the two samples are in good agreement at high energy. The plausible interpretation of the flux supports strongly the view that extragalactic high-energy cosmic neutrinos have been observed. This emission is *diffuse* emission: probably, this diffuse emission is, at least in part, due simply to *still unresolved* emission.

Although smaller than IceCube, the ANTARES detector studied the diffuse emission from the Southern sky using both track- and shower-like events. They found, using data collected in nine years, a mild excess of high-energy events over the expected background; the excess is compatible with the IceCube findings [114].

The distribution that fits the data-set of passing-events collected, Equation (28), fits also the high energy subset of the HESE, Equation (27); however the low energy part of the HESE does not agree with Equation (28). In order to explain the discrepancy, the hypothesis of an additional component present in the HESE, but not in the passing-event data-set, has been considered [115–118]. If (most of) the cosmic neutrinos have an extragalactic origin, an isotropic distribution is to be expected. This is in first approximation in agreement with the observations of IceCube. A contribution due to a Milky Way emission cannot be excluded, and a value of the order of $\sim$ 10% at $E_\nu > 60$ TeV is not incompatible with observations [93].

The identification of sources of the high energy neutrinos relies on the possible correlation of observed events with specific objects in the sky and/or by self-correlating the events themselves. A part with the relevant exception of the coincidence between the direction of a very-high energy ν_μ and the position of a blazar, as discussed in Section 7.3, searches of correlations among neutrino candidates and classes of astrophysical objects contained in gamma-ray catalogs did not reveal a significant amount of coincidences [107,119,120].

From theoretical models, the timescale of the neutrino emission depends dramatically upon the type of sources. The hypothesis that the gamma ray burst are associated to a prompt neutrino emission (lasting a few hours or less) has been tested: the non-detection of coincident events between neutrinos and GRBs with IceCube [121,122] and ANTARES [123] data has led to important constraints on cosmic-ray acceleration in GRBs. Other episodic events of intense neutrino emission could at least in principle occur in AGN, and be associated, for example, also to accretion phenomena. On the contrary, it is unlikely that stationary populations of cosmic rays (as, say, the ones that presumably exist in a starburst galaxy) may lead to this type of phenomenology.

The current status of experimental results is not inconsistent with expectations, namely that there exist astronomical sites where cosmic rays distributed as $E_{\rm CR}^{-2}$ collide with surrounding hadrons leading to intense neutrino fluxes, whose distribution reflects closely the cosmic ray spectra. However, it is quite evident the interest in probing accurately the shape and the extent of the observed spectrum, checking it at very high energies, observing events at the Glashow resonance energy, tau neutrinos.

A key role will be also the observation of cosmic events below few tens of TeV against the background of atmospheric events, using the improved angular resolution of incoming detectors. In the quest for the identification of (some of) the sources, the muon events (that induced by ν_μ CC interactions) have the best angular resolution and offer the best chances. The improved angular resolution is one one of the main motivation for large volume neutrino telescope in water, as foreseen by the KM3NeT project. Other reasons are the need to verify the current findings/discoveries and the wish to explore new patches of the sky - including the central regions of the Milky Way. Last but not least, when reliable observational information will be available, it will be possibly to study interesting and possibly important sites for cosmic ray production and the environment where they interact. For this, the role of Multimessenger astronomy is of paramount importance.

Author Contributions: Conceptualization, F.V.; Methodology, F.V., M.S.; Software, A.P., M.S.; Investigation, A.P., M.S.; Validation, all; Writing—Original Draft Preparation, F.V., M.S.; Writing—Review & Editing, all. All authors have read and agreed to the published version of the manuscript.

Funding: This work was partially supported by the research grant number 2017W4HA7S "NAT-NET: Neutrino and Astroparticle Theory Network" under the program PRIN 2017 funded by the Italian Ministero dell'Istruzione, dell'Università e della Ricerca (MIUR); it has received funding from the European Research Council (ERC) under the European Union's Horizon 2020 research and innovation programme (Grant No. 646623). Figures 6 and 13 are reproduced by permission of IOP Publishing: ©IOP Publishing Ltd and Sissa Medialab, all rights reserved.

Acknowledgments: We are grateful to three anonymous reviewers for the excellent feedback we received. F.V. thanks F. Aharonian, A. Capone, S. Celli, M.L. Costantini, E. Esmaili, A. Gallo Rosso, P.L. Ghia, C. Mascaretti, E. Roulet and V. Zema for precious discussions.

Conflicts of Interest: The authors declare no conflict of interest.

Appendix A. How to Estimate Neutrinos from Gamma-Rays

After the discussion and the caveats, we give various practical recipes to connect high energy gamma rays and neutrinos: In order, to be definite we focus on pp collisions and quantify the connection between neutrinos and gamma rays in various levels of approximation.

(i) The simplest procedure is just to recall that the leading pion carries about 1/5 of the initial proton, and that the energy partition in its subsequent decay leads to a similar sharing of energy. Therefore, each neutrino carries about 1/20 of the initial proton energy whereas the gamma rays (from neutral pion) have twice this energy.

(ii) A very practical recipe, that can be adopted in the case when the cosmic ray spectra obey the exponential cutoff distribution, is the following one [124]

$$\frac{dN_p}{dE} = A_p E^{-\alpha} \exp\left(-\frac{E}{\epsilon_p}\right) \Rightarrow \frac{dN_{\gamma/\nu}}{dE} = A_{\gamma/\nu} E^{-\Gamma_{\gamma/\nu}} \exp\left(-\sqrt{\frac{E}{\epsilon_{\gamma/\nu}}}\right)$$

where

$$A_\nu \approx (0.71 - 0.16\alpha)A_\gamma, \;\; \Gamma_\nu \approx \Gamma_\gamma \approx \alpha - 0,1, \;\; \epsilon_\nu \approx 0.59\epsilon_\gamma \approx \epsilon_p/40$$

In this approximation, all neutrinos have the same spectrum, mostly due to oscillations.

(*iii*) Finally an accurate approximation allows us to find the neutrino flux F_ν from the gamma ray flux F_γ in the same assumptions, simply by performing one integral with a known kernel that accounts for the kinematics of the decay as shown in Reference [125], based on the results of Reference [30], and as further improved in Reference [40]. For example, the sum of the muon neutrinos and antineutrinos is given by

$$\Phi_{\nu_\mu}(E_\nu) + \Phi_{\bar{\nu}_\mu}(E_\nu) = 0.66\,\Phi_\gamma\left(\frac{E_\nu}{1-r_\pi}\right) + 0.02\,\Phi_\gamma\left(\frac{E_\nu}{1-r_K}\right) + \int_0^1 \kappa(x)\;\Phi_\gamma\left(\frac{E_\nu}{x}\right)dx$$

where the first term comes from pion decay ($r_\pi = (m_\mu/m_\pi)^2$), the second from kaon decay ($r_K = (m_\mu/m_K)^2$), the third from the muons, and

$$\kappa(x) = \begin{cases} x^2(33.8 - 54.3x), & \text{if } x < r_K \\ (1-x)^2(-0.63 + 12.45x), & \text{if } x > r_\pi \\ 0.04 + 0.20x + 7.44x^2 - 7.53x^3 & \text{otherwise} \end{cases}$$

See Reference [48] for the other flavors and for the most updated expression of the kernels. Note that in the last method, the assumption of a power law distribution is not necessary. Of course, in all of these cases the gamma ray flux is supposed to be fully due to 'hadronic' origin and to be unperturbed from propagation, as discussed just above.

References

1. Greisen, K. Cosmic ray showers. *Ann. Rev. Nucl. Part Sci.* **1960**, *10*, 63. [CrossRef]
2. Markov, M.A.; Zheleznykh, I.M. On high energy neutrino physics in cosmic rays. *Nucl. Phys.* **1961**, *27*, 385. [CrossRef]
3. Zheleznykh, I.M. Early years of high-energy neutrino physics in cosmic rays and neutrino astronomy (1957–1962). *Int. J. Mod. Phys. A* **2006**, *21*, 1. [CrossRef]
4. Morrison, P. On Gamma-Ray Astronomy. *Il Nuovo Cimento Vol VII* **1958**, *6*, 858. [CrossRef]
5. Reines, F.; Kropp, W.R.; Sobel, H.W.; Gurr, H.S.; Lathrop, J.; Crouch, M.F.; Sellschop, J.P.F.; Meyer, B.S. Muons produced by atmospheric neutrinos: Experiment. *Phys. Rev. D* **1971**, *4*, 80. [CrossRef]
6. Chen, H.H.; Kropp, W.R.; Sobel, H.W.; Reines, F. Muons produced by atmospheric neutrinos: Analysis. *Phys. Rev. D* **1971**, *4*, 99. [CrossRef]
7. Krishnaswamy, M.R.; Menon, M.G.K.; Narasimham, V.S.; Hinotani, K.; Ito, N.; Miyake, S.; Osborne, J.L.; Parsons, A.J.; Wolfendale, A.W. The Kolar Gold Fields Neutrino Experiment. 1. the Interactions of Cosmic Ray Neutrinos. *Proc. R. Soc. Lond. A* **1971**, *323*, 489.
8. Aartsen, M.G.; Abbasi, R.; Abdou, Y.; Ackermann, M.; Adams, J.; Aguilar, J.A.; Ahlers, M.; Altmann, D.; Auffenberg, J.; Bai, X.; et al. [IceCube Collaboration]. First observation of PeV-energy neutrinos with IceCube. *Phys. Rev. Lett.* **2013**, *111*, 021103. [CrossRef]
9. Suzuki, A.; Koshiba, M. History of neutrino telescope/astronomy. *Exper. Astron.* **2009**, *25*, 209. [CrossRef]
10. Spiering, C. Towards High-Energy Neutrino Astronomy. A Historical Review. *Eur. Phys. J. H* **2012**, *37*, 515. [CrossRef]
11. Proceedings of the International Conference on History of the Neutrino: 1930–2018. Available online: Http://inspirehep.net/record/1760351 (accessed on 8 February 2020).
12. Pontecorvo, B. Neutrino Experiments and the Problem of Conservation of Leptonic Charge. *Sov. Phys. JETP* **1968**, *26*, 984.
13. The Nobel Prize in Physics 2015. Available online: https://www.nobelprize.org/prizes/physics/2015/ (accessed on 30 December 2019).

14. Spurio, M. Probes of Multimessenger Astrophysics - Charged cosmic rays, neutrinos, γ-rays and gravitational waves. Springer: Cham, Switzerland, 2018.
15. Capone, A.; Lipari, P.; Vissani, F. Neutrino Astronomy. In *Multiple Messengers and Challenges in Astroparticle Physics*; Aloisio, R., Coccia, E., Vissani, F., Eds.; Springer: Cham, Switzerland, 2018.
16. Halzen, F.; Hooper, D. High-energy neutrino astronomy: The Cosmic ray connection. *Rept. Prog. Phys.* **2002**, *65*, 1025.
17. Lipari, P. Proton and Neutrino Extragalactic Astronomy. *Phys. Rev. D* **2008**, *78*, 083011.
18. Chiarusi, T.; Spurio, M. High-Energy Astrophysics with Neutrino Telescopes. *Eur. Phys. J. C* **2010**, *65*, 649.
19. Waxman, E. Neutrino astrophysics: A new tool for exploring the universe. *Science* **2007**, *315*, 63.
20. DeYoung, T. Neutrino Astronomy with IceCube. *Mod. Phys. Lett.* **2009**, *A24*, 1543.
21. Anchordoqui, L.A.; Montaruli, T. In Search for Extraterrestrial High Energy Neutrinos. *Ann. Rev. Nucl. Part Sci.* **2010**, *60*, 129.
22. Katz, U.F.; Spiering, C. High-Energy Neutrino Astrophysics: Status and Perspectives. *Prog. Part. Nucl. Phys.* **2012**, *67*, 651. [CrossRef]
23. Gallo Rosso, A.; Mascaretti, C.; Palladino, A.; Vissani, F. Introduction to neutrino astronomy. *Eur. Phys. J. Plus* **2018**, *133*, 267. [CrossRef]
24. Berezinsky, V.S.; Bulanov, S.V.; Ginzburg, V.L.; Dogiel, V.A.; Ptuskin, V.S. Astrophysics of Cosmic Rays; North-Holland: Amsterdam, The Netherlands, 1990.
25. Gaisser, T.K.; Engel, R.; Resconi, E. *Cosmic Rays and Particle Physics*; Cambridge University Press: Cambridge, UK, 2016.
26. Stecker, F.W. Cosmic Physics: The High Energy Frontier. *J. Phys. G* **2003**, *29*, R47.
27. Matthiae, G. The cosmic ray energy spectrum as measured using the Pierre Auger Observatory. *New J. Phys.* **2010**, *12*, 075009. [CrossRef]
28. Berezinsky, V.S.; Volynsky, V.V. Generation Function Of High-energy Cosmic Neutrinos. I. PP-Neutrino. Available online: Http://adsabs.harvard.edu/full/1979ICRC...10..326B (accessed on 6 February 2020).
29. Kelner, S.K.; Aharonian, F.A.; Bugayov, V.V. Energy spectra of gamma-rays, electrons and neutrinos produced at proton-proton interactions in the very high energy regime. *Phys. Rev. D* **2006**, *74*, 034018. [CrossRef]
30. Volkova, L.V. Energy Spectra and Angular Distributions of Atmospheric Neutrinos.*Sov. J. Nucl. Phys.* **1980**, *31*, 784.
31. Rybicki, G.B.; Lightman, A.P. *Radiative Processes in Astrophysics*; Wiley-VCH Pub.: Hoboken, NJ, USA, 1991.
32. Yen, E. New scaling variable and early scaling in single-particle inclusive distributions for hadron-hadron collisions. *Phys. Rev. D* **1974**, *10*, 836. [CrossRef]
33. Allard, D. Extragalactic propagation of ultrahigh energy cosmic-rays. *Astropart. Phys.* **2012**, *33*, 39–40. [CrossRef]
34. Celli, S.; Palladino, A.; Vissani, F. Neutrinos and γ-rays from the Galactic Center Region after H.E.S.S. multi-TeV measurements. *Eur. Phys. J. C* **2017**, *77*, 66. [CrossRef]
35. Simple Quantum Integro Differential Solver (SQiIDS). Available online: http://www.lns.mit.edu/~caad/software.html (accessed on 30 December 2019).
36. Aharonian, F.; O'Drury, L.; Volk, H.J. GeV/TeV gamma-ray emission from dense molecular clouds overtaken by supernova shells. *Astron. Astroph.* **1994**, *285*, 645.
37. Drury, L.O.; Aharonian, F.A.; Volk, H.J. The Gamma-ray visibility of supernova remnants: A Test of cosmic ray origin. *Astron. Astrophys.* **1994**, *287*, 959.
38. Naito, T.; Takahara, F. High-energy gamma-ray emission from supernova remnants. *J. Phys. G* **194**, *20*, 477. [CrossRef]
39. Alvarez-Muniz, J.; Halzen, F. Possible high-energy neutrinos from the cosmic accelerator RX J1713.7-3946. *Astrophys. J.* **2002**, *576*, L33. [CrossRef]
40. Villante, F.L.; Vissani, F. How precisely neutrino emission from supernova remnants can be constrained by gamma ray observations? *Phys. Rev. D* **2008**, *78*, 103007. [CrossRef]
41. Vissani, F.; Aharonian, F.; Sahakyan, N. On the Detectability of High-Energy Galactic Neutrino Sources. *Astropart. Phys.* **2011**, *34*, 778. [CrossRef]
42. Aiello, S.; et al. [The KM3NeT collaboration]. Sensitivity of the KM3NeT/ARCA neutrino telescope to point-like neutrino sources. *Astropart. Phys.* **2019**, *111*, 100–110. [CrossRef]
43. Gribov, V.N.; Pontecorvo, B. Neutrino astronomy and lepton charge. *Phys. Lett. B* **1969**, *28*, 493. [CrossRef]

44. Berezinsky, V.S.; Gazizov, A.Z. Cosmic neutrino and the possibility of Searching for W bosons with masses 30-100 GeV in underwater experiments. *JETP Lett.* **1977**, *25*, 254.
45. Bilenky, S.M.; Pontecorvo, B. Lepton Mixing and Neutrino Oscillations. *Phys. Rept.* **1978**, *41*, 225. [CrossRef]
46. Esteban, I.; Gonzalez-Garcia, M.C.; Hernandez-Cabezudo, A.; Maltoni, M.; Schwetz, T. Global analysis of three-flavour neutrino oscillations: Synergies and tensions in the determination of θ_{23}, δ_{CP}, and the mass ordering. *J. High Energy Phys.* **2019**, *1901*, 106. [CrossRef]
47. Palladino, A.; Vissani, F. The natural parameterization of cosmic neutrino oscillations. *Eur. Phys. J. C* **2015**, *75*, 433. [CrossRef]
48. Mascaretti, C.; Vissani, F. On the relevance of prompt neutrinos for the interpretation of the IceCube signals. *J. Cosmol. Astropart. Phys.* **2019**, *1908*, 004. [CrossRef]
49. Palladino, A.; Mascaretti, C.; Vissani, F. The importance of observing astrophysical tau neutrinos. *J. Cosmol. Astropart. Phys.* **2018**, *1808*, 004. [CrossRef]
50. Bugaev, E.; Montaruli, T.; Shlepin, Y.; Sokalski, I. Propagation of tau neutrinos and tau leptons through the Earth and their detection in underwater/ice neutrino telescopes. *Astropart. Phys.* **2004**, *21*, 491–509. [CrossRef]
51. Dziewonski, A.M.; Anderson. D.L. Preliminary reference Earth model. *Phys. Earth Planet. Inter.* **1981**, *25*, 297–356. [CrossRef]
52. Murase, K.; Bartos, I. High-Energy Multimessenger Transient Astrophysics. *Ann. Rev. Nucl. Part. Sci.* **2019**, *69*, 477. [CrossRef]
53. Halzen, F.; Kheirandish, A. Multimessenger Search for the Sources of Cosmic Rays Using Cosmic Neutrinos. *Front. Astron. Space Sci.* **2019**, *6*, 32. [CrossRef]
54. Achterberg, A.; et al. [IceCube Collaboration]. First Year Performance of The IceCube Neutrino Telescope. *Astropart. Phys.* **2006**, *26*, 155–173. [CrossRef]
55. Aartsen, M.G.; et al. [IceCube Collaboration]. The Design and Performance of IceCube DeepCore. *Astropart. Phys. 2012*, *35*, 615.
56. Aartsen, M.G.; et al. [IceCube Collaboration]. The IceCube Neutrino Observatory: Instrumentation and Online Systems. *J. Instrum.* **2017**, *12*, P03012. [CrossRef]
57. Ageron, M.; et al. [ANTARES Collaboration]. ANTARES: The first undersea neutrino telescope. *Nucl. Instrum. Meth.* **2011**, *A656*, 11. [CrossRef]
58. Albert, A.; et al. [ANTARES Collaboration]. Long-term monitoring of the ANTARES optical module efficiencies using 40K decays in sea water. *Eur. Phys. J. C* **2018**, *78*, 669. [CrossRef]
59. Adrián-Martínez, S.; Ageron, M.; Aharonian, F.; Aiello, S.; Ameli, F.; Anassontzis, E.; Andre, M.; Androulakis, G.; Anghinolfi, M.; et al. Letter of intent for KM3NeT 2.0. *J. Phys. G Nucl. Part. Phys.* **2016**, *43*, 084001. [CrossRef]
60. Adrián-Martínez, S.; et al. [The KM3NeT collaboration]. Intrinsic limits on resolutions in muon- and electron-neutrino charged-current events in the KM3NeT/ORCA detector. *J. High Energy Phys.* **2017**, **5**, 8.
61. Aynutdinov, V.; Avrorin, V.A.; Aynutdinov, V.M.; Bannasch, R.; Belolaptikov, I.A.; Bogorodsky, D.Yu.; Brudanin, V.B.; Budnev, N.M.; Danilchenko, I.A.; Domogatsky, G.V.; et al. The prototyping/early construction phase of the BAIKAL-GVD project. *Nucl. Instrum. Methods Phys. Res. Sect. A* **2014**, *742*, 82–88.
62. Avrorin, A.D.; et al. [Baikal-GVD Collaboration]. Search for cascade events with Baikal-GVD. Available online: Https://arxiv.org/abs/1908.05430 (accessed on 6 February 2020).
63. Learned, J.G.; Pakvasa, S. Detecting Nutau Oscillations as PeV Energies. *Astropart. Phys.* **1995**, *3*, 267. [CrossRef]
64. Aartsen, M.G.; et al. [IceCube Collaboration]. Search for high-energy neutrinos from gravitational wave event GW151226 and candidate LVT151012 with ANTARES and IceCube. *Phys. Rev. D* **2016**, *93*, 022001. [CrossRef]
65. Glashow, S.L. Resonant Scattering of Antineutrinos. *Phys. Rev.* **1960**, *118*, 316. [CrossRef]
66. Palladino, A.; Pagliaroli, G.; Villante, F.L.; Vissani, F. Double pulses and cascades above 2 PeV in IceCube. *Eur. Phys. J. C* **2016**, *76*, 52 . [CrossRef]
67. Gandhi, R.; Quigg, C.; Reno, M.H.; Sarcevic, I. Ultrahigh-energy neutrino interactions. *Astropart. Phys.* **1996**, *5*, 81. [CrossRef]
68. Abbasi, R. et al. [IceCube Collaboration]. Measurement of the atmospheric neutrino energy spectrum from 100 GeV to 400 TeV with IceCube. *Phys. Rev. D* **2011**, *83*, 012001. [CrossRef]

69. Adrian-Martinez, S.; et al. [ANTARES Collaboration]. Measurement of the atmospheric ν_μ energy spectrum from 100 GeV to 200 TeV with the ANTARES telescope. *Eur. Phys. J. C* **2013**, *73*, 2606. [CrossRef]
70. Aartsen, M.G.; et al. [IceCube Collaboration]. Measurement of the Atmospheric ν_e Spectrum with IceCube. *Phys. Rev. D* **2015**, *91*, 122004. [CrossRef]
71. Aartsen, M.G.; et al. [IceCube Collaboration]. Characterization of the Atmospheric Muon Flux in IceCube. *Astropart. Phys.* **2016**, *78*, 1. [CrossRef]
72. Aiello, S.; et al. [NEMO Collaboration]. Measurement of the atmospheric muon depth intensity relation with the NEMO Phase-2 tower. *Astropart. Phys.* **2015**, *66*, 1. [CrossRef]
73. Aguilar, J.A.; et al. [ANTARES Collaboration]. Zenith distribution and flux of atmospheric muons measured with the 5-line ANTARES detector. *Astropart. Phys.* **2010**, *34*, 179. [CrossRef]
74. Adrián-Martínez, S.; et al. [ANTARES Collaboration]. Time calibration with atmospheric muon tracks in the ANTARES neutrino telescope. *Astropart. Phys.* **2016**, *78*, 43.
75. Becherini, Y.; Margiotta, A.; Sioli, M.; Spurio, M. A Parameterisation of single and multiple muons in the deep water or ice. *Astropart. Phys.* **2006**, *25*, 1–13. [CrossRef]
76. Schönert, S.; Gaisser, T.K.; Resconi, E.; Schulz, O. Vetoing atmospheric neutrinos in a high energy neutrino telescope. *Phys. Rev. D* **2009**, *79*, 043009. [CrossRef]
77. Argüelles, C.A.; Palomares-Ruiz, S.; Schneider, A.; Wille, L.; Yuan, T. Unified atmospheric neutrino passing fractions for large-scale neutrino telescopes. *J. Cosmol. Astropart. Phys.* **2018**, *1807*, 047.
78. Gaisser, T.K.; Jero, K.; Karle, A.; van Santen, J. Generalized self-veto probability for atmospheric neutrinos. *Phys. Rev.* **2014**, *D90*, 023009. [CrossRef]
79. Halzen, F. IceCube: Opening a new window on the universe from the South Pole. *Int. J. Mod. Phys. D* **2018**, *28*, 1930007. [CrossRef]
80. Ahlers, M.; Halzen, F. Opening a New Window onto the Universe with IceCube. *Prog. Part Nucl. Phys.* **2018**, *102*, 73. [CrossRef]
81. Aartsen, M.G.; et al. [IceCube Collaboration]. Evidence for high-energy extraterrestrial neutrinos at the IceCube detector. *Science* **2013**, *342*, 1242856. [PubMed]
82. Aartsen, M.G. et al. [IceCube Collaboration]. Flavor Ratio of Astrophysical Neutrinos above 35 TeV in IceCube. *Phys. Rev. Lett.* **2015**, *114*, 171102. [CrossRef] [PubMed]
83. Schneider, A. [The IceCube Collaboration]. Characterization of the Astrophysical Diffuse Neutrino Flux with IceCube High-Energy Starting Events. Available online: Https://arxiv.org/abs/1907.11266 (accessed on 6 February 2020).
84. Aartsen, M.G.; et al. [IceCube Collaboration]. Evidence for Astrophysical Muon Neutrinos from the Northern Sky with IceCube. *Phys. Rev. Lett.* **2015**, *115*, 081102. [CrossRef] [PubMed]
85. Aartsen, M.G.; et al. [IceCube Collaboration]. Observation and Characterization of a Cosmic Muon Neutrino Flux from the Northern Hemisphere using six years of IceCube data. *Astrophys. J.* **2016**, *833*, 3. [CrossRef]
86. Stettner, J. [The IceCube Collaboration]. Measurement of the Diffuse Astrophysical Muon-Neutrino Spectrum with Ten Years of IceCube Data. Available online: Https://arxiv.org/abs/1908.09551 (accessed on 6 February 2020).
87. Paiano, S.; Falomo, R.; Treves, A.; Scarpa, R. The redshift of the BL Lac object TXS 0506+056. *Astrop. J.* **2018**, *854*, L32. [CrossRef]
88. Aartsen, M.G.; et al. [IceCube and Fermi-LAT and MAGIC and AGILE and ASAS-SN and HAWC and H.E.S.S. and INTEGRAL and Kanata and Kiso and Kapteyn and Liverpool Telescope and Subaru and Swift NuSTAR and VERITAS and VLA/17B-403 Collaborations]. Multimessenger observations of a flaring blazar coincident with high-energy neutrino IceCube-170922A. *Science* **2018**, *361*, 6398.
89. Aartsen, M.G.; et al. [IceCube Collaboration]. Neutrino emission from the direction of the blazar TXS 0506+056 prior to the IceCube-170922A alert. *Science* **2018**, *361*, 147.
90. Albert, A.; et al. [ANTARES Collaboration]. The Search for Neutrinos from TXS 0506+056 with the ANTARES Telescope. *Astrophys. J.* **2018**, *863*, L30. [CrossRef]
91. Albert, A.; et al. [ANTARES Collaboration]. First all-flavor neutrino pointlike source search with the ANTARES neutrino telescope. *Phys. Rev. D* **2017**, *96*, 082001. [CrossRef]
92. Albert, A.; et al. [ANTARES and IceCube Collaborations]. ANTARES and IceCube Combined Search for Neutrino Point-like and Extended Sources in the Southern Sky. *arXiv* **2020**, arXiv:2001.04412.

93. Albert, A.; et al. [ANTARES and IceCube Collaborations].Joint Constraints on Galactic Diffuse Neutrino Emission from the ANTARES and IceCube Neutrino Telescopes. *Astrophys. J. Lett.* **2018**, *86*, L20. [CrossRef]
94. Murase, K.; Waxman, E. Constraining High-Energy Cosmic Neutrino Sources: Implications and Prospects. *Phys. Rev. D* **2016**, *94*, 103006. [CrossRef]
95. GCN: The Gamma-Ray Coordinates Network. Available online: Https://gcn.gsfc.nasa.gov/ (accessed on 30 December 2019).
96. Urry, C.M.; Padovani, P. Unified schemes for radio-loud active galactic nuclei. *Publ. Astron. Soc. Pac.* **1995**, *107*, 803. [CrossRef]
97. Stecker, F.W.; Done, C.; Salamon, M.H.; Sommers, P. High-energy neutrinos from active galactic nuclei. *Phys. Rev. Lett.* **1991**, *66*, 2697. [CrossRef]
98. Stecker, F.W. PeV neutrinos observed by IceCube from cores of active galactic nuclei. *Phys. Rev. D* **2013**, *88*, 047301. [CrossRef]
99. Kalashev, O.; Semikoz, D.; Tkachev, I. Neutrinos in IceCube from active galactic nuclei. *J. Exp. Theor. Phys.* **2015**, *120*, 541. [CrossRef]
100. Boettcher, M.; Reimer, A.; Sweeney, K.; Prakash, A. Leptonic and Hadronic Modeling of Fermi-Detected Blazars. *Astrophys. J.* **2013**, *768*, 54. [CrossRef]
101. Ackermann, M.; et al. [Fermi-LAT Collaboration]. Resolving the Extragalactic γ-Ray Background above 50 GeV with the Fermi Large Area Telescope. *Phys. Rev. Lett.* **2016**, *116*, 151105. [CrossRef]
102. Keivani, A.; Murase, K.; Petropoulou, M.; Fox, D.B.; Cenko, S.B.; Chaty, S.; Coleiro, A.; DeLaunay, J.J.; Dimitrakoudis, S.; Evans, P.A.; et al. A Multimessenger Picture of the Flaring Blazar TXS 0506+056: Implications for High-Energy Neutrino Emission and Cosmic Ray Acceleration. *Astrophys. J.* **2018**, *864*, 84. [CrossRef]
103. Murase, K.; Oikonomou, F.; Petropoulou, M. Blazar Flares as an Origin of High-Energy Cosmic Neutrinos? *Astrophys. J.* **2018**, *865*, 124. [CrossRef]
104. Palladino, A.; Rodrigues, X.; Gao, S.; Winter, W. Interpretation of the diffuse astrophysical neutrino flux in terms of the blazar sequenc. *Astrophys. J.* **2019**, *871*, 41. [CrossRef]
105. Kadler, M.; Krauß, F.; Mannheim, K.; Ojha, R.; Müller, C.; Schulz, R.; Anton, G.; Baumgartner, W.; Beuchert, T.; Buson, S.; et al. Coincidence of a high-fluence blazar outburst with a PeV-energy neutrino event. *Nat. Phys.* **2016**, *12*, 807. [CrossRef]
106. Murase, K.; Inoue, Y.; Dermer, C.D. Diffuse Neutrino Intensity from the Inner Jets of Active Galactic Nuclei: Impacts of External Photon Fields and the Blazar Sequence. *Phys. Rev. D* **2014**, *90*, 023007. [CrossRef]
107. Padovani, P.; Resconi, E.; Giommi, P.; Arsioli, B.; Chang, Y.L. Extreme blazars as counterparts of IceCube astrophysical neutrinos. *Mon. Not. R. Astron. Soc.* **2016**, *457*, 3582. [CrossRef]
108. Ackermann, M.; Ahlers, M.; Anchordoqui, L.; Bustamante, M.; Connolly, A.; Deaconu, C.; Grant, D.; Gorham, P.; Halzen, F.; Karle, A.; et al. Astrophysics Uniquely Enabled by Observations of High-Energy Cosmic Neutrinos. *Bull. Am. Astron. Soc.* **2019**, *51*, 185.
109. Tamborra, I.; Ando, S.; Murase, K. Star-forming galaxies as the origin of diffuse high-energy backgrounds: Gamma-ray and neutrino connections, and implications for starburst history. *J. Cosmol. Astropart. Phys.* **2014**, *1409*, 043. [CrossRef]
110. Chang, X.C.; Wang, X.Y. The diffuse gamma-ray flux associated with sub-PeV/PeV neutrinos from starburst galaxies. *Astrophys. J.* **2014**, *793*, 131. [CrossRef]
111. Loeb, A.; Waxman, E. The Cumulative background of high energy neutrinos from starburst galaxies. *J. Cosmol. Astropart. Phys.* **2006**, *0605*, 003. [CrossRef]
112. Bechtol, k.; Ahlers, M.; Di Mauro, M.; Ajello, M.; Vandenbroucke, J. Evidence against star-forming galaxies as the dominant source of IceCube neutrinos. *Astrophys. J.* **2017**, *836*, 47. [CrossRef]
113. Palladino, A.; Fedynitch, A.; Rasmussen, R.W.; Taylor, A.M. IceCube Neutrinos from Hadronically Powered Gamma-Ray Galaxies. *J. Cosmol. Astropart. Phys.* **2019**, *1909*, 004. [CrossRef]
114. Albert, A.; et al. [ANTARES Collaborations]. All-flavor Search for a Diffuse Flux of Cosmic Neutrinos with Nine Years of ANTARES Data. *Astrophys. J. Lett.* **2018**, *853*, L7. [CrossRef]
115. Spurio, M. Constraints to a Galactic Component of the Ice Cube cosmic neutrino flux from ANTARES. *Phys. Rev. D* **2014**, *90*, 103004. [CrossRef]
116. Chen, C.-Y.; Bhupal Dev, P.S.; Soni, A. Two-component flux explanation for the high energy neutrino events at IceCube. *Phys. Rev. D* **2015**, *92*, 073001. [CrossRef]

117. Palladino, A.; Vissani, F. Extragalactic plus Galactic model for IceCube neutrino events. *Astrophys. J.* **2016**, *826*, 185. [CrossRef]
118. Vincent, A.C.; Palomares-Ruiz, S.; Mena, O. Analysis of the 4-year IceCube high-energy starting events. *Phys. Rev.* **2016**, *D94*, 023009. [CrossRef]
119. Aartsen, M.G.; et al. [IceCube Collaboration]. The contribution of Fermi-2LAC blazars to the diffuse TeV-PeV neutrino flux. *Astrophys. J.* **2017**, *835*, 45. [CrossRef]
120. Palladino, A.; Vissani, F. Can BL Lacertae emission explain the neutrinos above 0.2 PeV? *Astron. Astrophys.* **2017**, *604*, A18. [CrossRef]
121. Abbasi, R.; et al. [IceCube Collaboration] An absence of neutrinos associated with cosmic-ray acceleration in γ-ray bursts. *Nature* **2012**, *484*, 351.
122. Aartsen, M.G.; et al. [IceCube Collaboration] Search for Prompt Neutrino Emission from Gamma-Ray Bursts with IceCube. *Astrophys. J.* **2015**, *805*, L5. [CrossRef]
123. Albert, A.; André, M.; Anghinolfi, M.; Anton, G.; Ardid, M.; Aubert, J.-J.; Avgitas, T.; Baret, B.; Barrios-Martí, J.; Basa, S.; et al. Search for high-energy neutrinos from bright GRBs with ANTARES. *Mon. Not. R. Astron. Soc.* **2017**, *469*, 906. [CrossRef]
124. Kappes, A.; Hinton, J.; Stegmann, C.; Aharonian, F.A. Potential Neutrino Signals from Galactic Gamma-Ray Sources. *Astrophys. J.* **2007**, *656*, 870. [CrossRef]
125. Vissani, F. Neutrinos from galactic sources of cosmic rays with known γ-ray spectra. *Astropart. Phys.* **2006**, *26*, 310. [CrossRef]



© 2020 by the authors. Licensee MDPI, Basel, Switzerland. This article is an open access article distributed under the terms and conditions of the Creative Commons Attribution (CC BY) license (http://creativecommons.org/licenses/by/4.0/).